Bridging the gap between spectroscopy and partonic observables:

Edward Shuryak

Center for Nuclear Theory, Stony Brook University

Based on summary
of 20+papers
with Ismail Zahed
2019-2026
book e-Print: 2601.15085

LC26 talk, June 2026

The book is very large
(even table of contents is 8 pages)
and highly technical (appendices)
so it cannot be presented in few lectures

QCD vacuum
topology, semiclassics

hadronic spectroscopy
multiquarks, Fermi statistics

Spectroscpy on LF
WF -> PDFs, FFs, GPDs

Project as a bridge

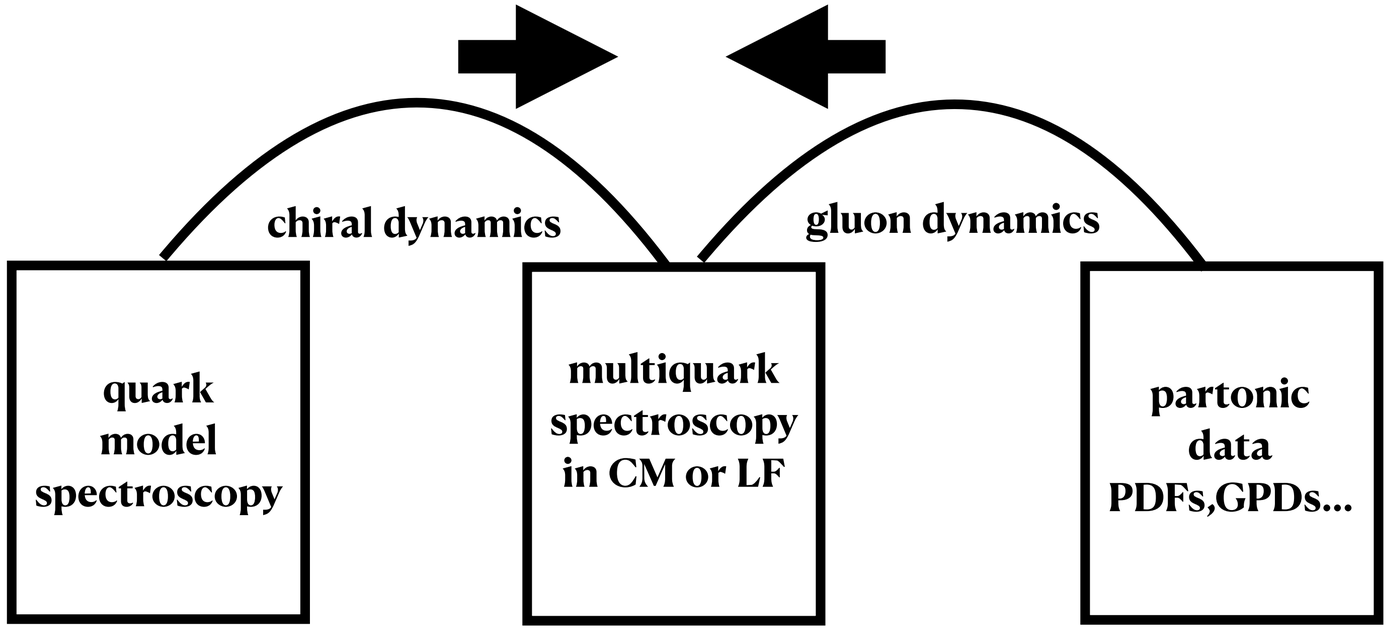

$Q^2 \sim \rho^{-2} \sim 0.4\,GeV^2$ $Q^2 \sim 1\,GeV^2$ $Q^2 \sim 4\,GeV^2$

Why repeat the QCD spectroscopy on the light front?

connection to partonic observables, DA, PDFs,GPDs, formfactors

in the rest frame, nonrelativistic approximation only works
if masses are much larger than momenta,
on the LF p_t^2 appear as a sum with m^2
and it does not matter which one is larger
=> same setting from Upsilons to light quark hadrons

$$m^2 \gg \vec{p}^2 \quad ?$$

kinetic energy on LF

$$\frac{p_{1\perp}^2 + m_Q^2}{x_1} + \frac{p_{2\perp}^2 + m_Q^2}{x_2} + \frac{p_{3\perp}^2 + m_Q^2}{x_3} =$$

Philosophy: start with "bare bone" LF Hamiltonian
constituent quarks + confinement
and solve it as accurate as possible,
with no arbitrary assumptions/approximations

no need for "CM motion subtraction

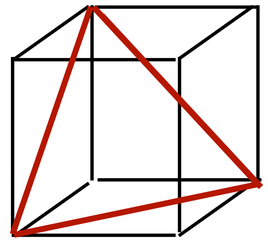

Jacobi coordinates

$$\vec{p}_{1\perp} = (\sqrt{6}\vec{p}_{\lambda\perp} + 3\sqrt{2}\vec{p}_{\rho\perp})/6, \qquad x_1 = (\sqrt{6}\lambda + 3\sqrt{2}\rho + 2X)/6$$
$$\vec{p}_{2\perp} = (\sqrt{6}\vec{p}_{\lambda\perp} - 3\sqrt{2}\vec{p}_{\rho\perp})/6, \qquad x_2 = (\sqrt{6}\lambda - 3\sqrt{2}\rho + 2X)/6$$
$$\vec{p}_{3\perp} = -\sqrt{6}\vec{p}_{\lambda\perp}/3 \qquad x_3 = (-\sqrt{6}\lambda + X)/3$$

$$X = x_1 + x_2 + x_3$$

longitudinal variables
are defined on equilateral triangle

The kinetic part of the LF Hamiltonian

$$\frac{p_{1\perp}^2 + m_Q^2}{x_1} + \frac{p_{2\perp}^2 + m_Q^2}{x_2} + \frac{p_{3\perp}^2 + m_Q^2}{x_3} =$$

$$3\sum_i (p_{i\perp}^2 + m_i^2) + \sum_i (p_{i\perp}^2 + m_i^2)\left(\frac{1}{x_i} - 3\right)$$

transverse
two 2d oscillators

non-factoriwable
"cup potential"

which is mostly zero
except near the edges
forcing LFWFs to vanish

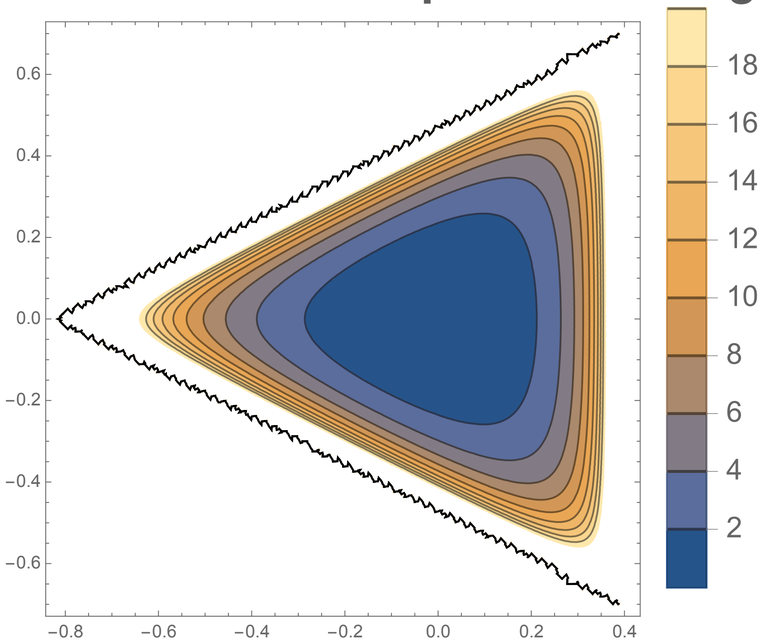

IG. 4. The contour plot of the "triangular cup" pote
tial $V(\lambda, \rho)$ on λ, ρ plot.

Confining Hamiltonian on LF can be desribed by:

Nambu-Goto string

$$S[\theta] = \int_0^T d\tau \sum_{i=1}^{3} \left(e_i m_i^2 + \frac{1}{4e_i} \dot{x}_i^2 \right) \qquad (37)$$
$$+\sigma_T \sum_{i=1}^{3} \int_0^T d\tau \int_0^1 d\sigma_i \sqrt{\dot{X}_i^2 X_i'^2 - (\dot{X}_i \cdot X_i')^2}$$

In momentum representation coordinates are derivatives, that is how we get a Laplacian

$$\to \int_0^T d\tau \left(3em_Q^2 + \frac{3}{4e} \right.$$
$$\left. + \frac{1}{4e} (\dot{r_\lambda}^2 + \dot{r_\rho}^2) + \sigma_T \sum_{i=1}^{3} |\xi_i(\theta)| \right)$$

the square root

$$\approx \sum_{i=1}^{3} \left(\frac{k_{i\perp}^2 + m_Q^2}{x_i} \right.$$
$$\left. + \sigma_T \left(3a + \frac{1}{a} \sum_{i=1}^{3} (|i\partial/\partial x_i|^2 + (3m_Q)^2 b_{i\perp}^2) \right) \right)$$

coord's are derivative over momenta

red triangles are Upsilon masses
from light front Hamiltonian

same method, 12*12 matrix diagonalized
higher states affected by a cutoff

note: orbital is not L but 2d m

Squared masses for n = 0..5 (left to right)
and orbital momentum m = 0,1,2 (down to up),
calculated from the light front Hamiltonian H_{LF}

usi
u
usin

(red triangles), and shifted by a constant, $M^2 - $ n+1
5 GeV ^2^2
the blue-circles show the squared masses M^2
calculated from Schroedinger

n+1

equation in the CM frame, with only linear plus
centrifugal potentials.

**Comparison between Upsilon masses
in Schreodinger CM frame with those from light front**

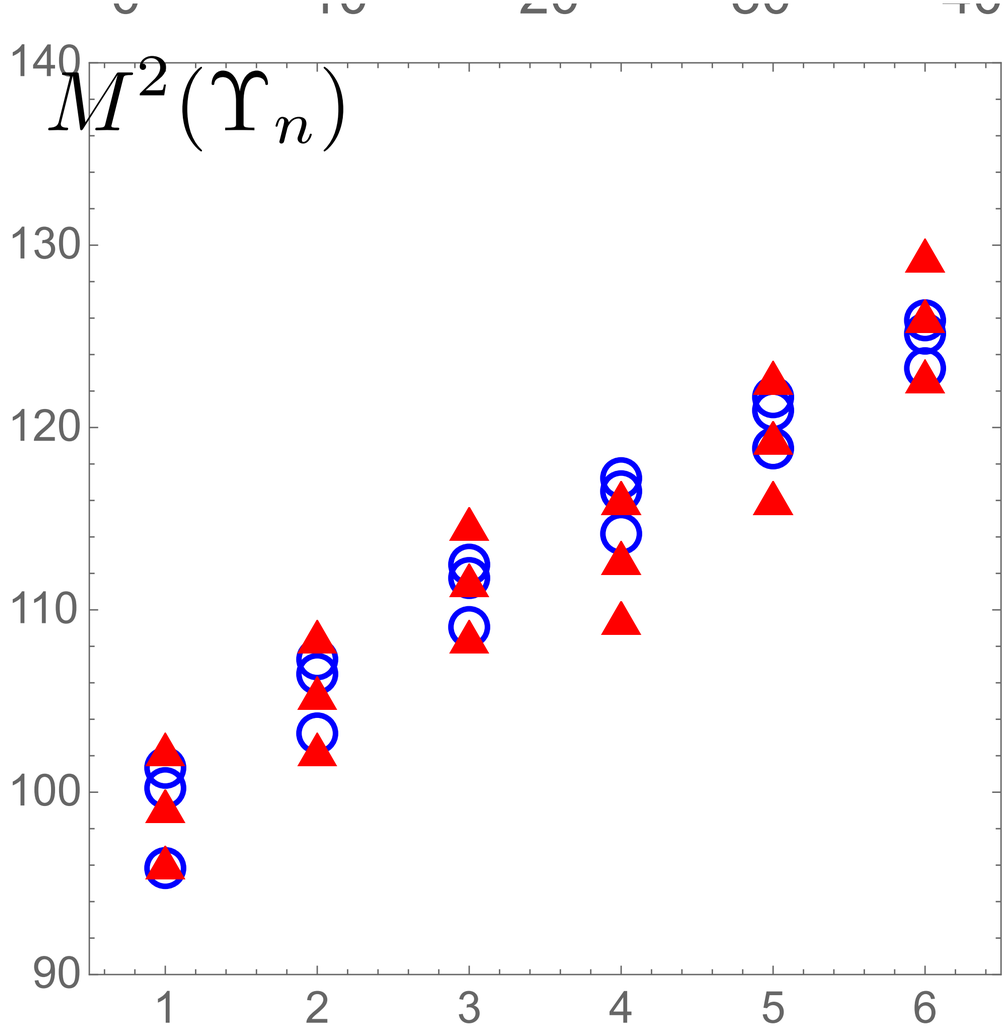

Philosophy: in momentum representation confinement produces derivative terms leading to Schreodinger-like equation

The Laplacian (which we encounter in the confining term of the Hamiltonian) in the original coordinates also takes a simple form

$$\nabla^2 = \sum_i \frac{\partial^2}{\partial x_i^2} \to \frac{\partial^2}{\partial \lambda^2} + \frac{\partial^2}{\partial \rho^2} + 3\frac{\partial^2}{\partial X^2} \qquad (31)$$

$$\varphi^{Dc}_{m,n}(\lambda,\rho) = \frac{4}{L\,3^{\frac{3}{4}}}\left[\cos\left(\frac{2\pi(2m_L-n_L)\rho}{3L}\right)\sin\left(\frac{2\pi n_L\tilde{\lambda}}{\sqrt{3}L}\right)\right.$$
$$-\cos\left(\frac{2\pi(2n_L-m_L)\rho}{3L}\right)\sin\left(\frac{2\pi m_L\tilde{\lambda}}{\sqrt{3}L}\right)$$
$$\left.+\cos\left(\frac{2\pi(m_L+n_L)\rho}{3L}\right)\sin\left(\frac{2\pi(m_L-n_L)\tilde{\lambda}}{\sqrt{3}L}\right)\right]$$
$$\varphi^{Ds}_{m,n}(\lambda,\rho) = \frac{4}{L\,3^{\frac{3}{4}}}\left[\sin\left(\frac{2\pi(2m_L-n_L)\rho}{3L}\right)\sin\left(\frac{2\pi n_L\tilde{\lambda}}{\sqrt{3}L}\right)\right.$$
$$-\sin\left(\frac{2\pi(2n_L-m_L)\rho}{3L}\right)\sin\left(\frac{2\pi m_L\tilde{\lambda}}{\sqrt{3}L}\right)$$
$$\left.-\sin\left(\frac{2\pi(m_L+n_L)\rho}{3L}\right)\sin\left(\frac{2\pi(m_L-n_L)\tilde{\lambda}}{\sqrt{3}L}\right)\right] \qquad (54)$$

with $\tilde{\lambda} = \lambda + L/\sqrt{3}$. Their symmetry properties include e.g. ρ mirror symmetry

$$\varphi^{Dc,s}(\lambda,-\rho) = +\varphi^{Dc,s}(\lambda,\rho) \qquad (55)$$

Full set of Eigenfunctions of the Laplacian on the equilateral triangle can be found both analytically (6 standing waves) and numerically with Mathematica

The Dirichlet states with $m_L = 2n_L$ are non-degenerate, with normalized eigenstates [14]

$$\varphi^{D}_{2n_L,n_L}(\lambda,\rho) =$$
$$\frac{2^{\frac{3}{2}}}{L\,3^{\frac{3}{4}}}\left[2\cos\left(\frac{2\pi n_L\rho}{L}\right)\sin\left(\frac{2\pi n_L\tilde{\lambda}}{\sqrt{3}L}\right) - \sin\left(\frac{4\pi n_L\tilde{\lambda}}{\sqrt{3}L}\right)\right]$$

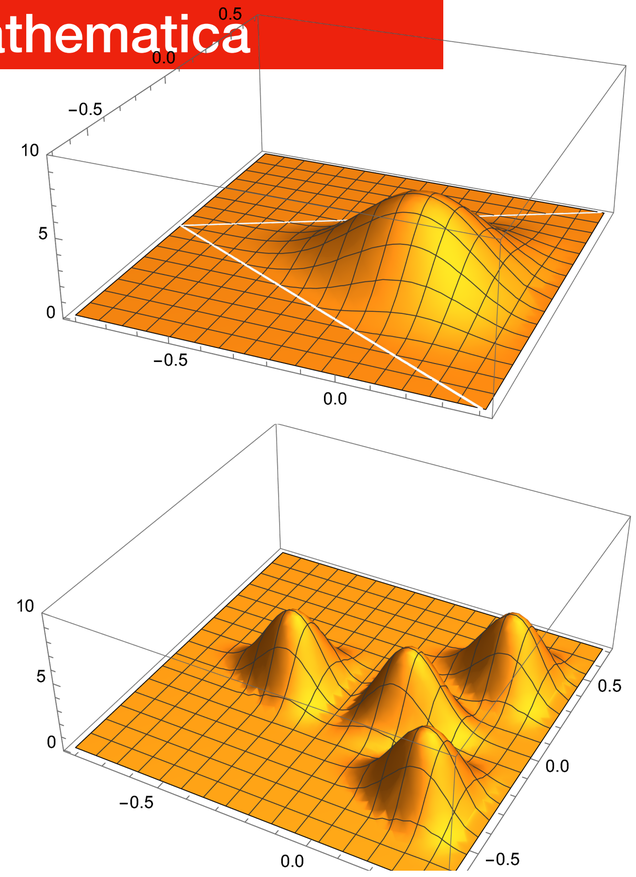

e-Print:s
2202.00167

Hadronic structure on the light-front IV. Heavy and light Baryons

$$H_{0LF} = 3(\vec{p}_\rho^{\,2} + \vec{p}_\lambda^{\,2} + 3m_Q^2)$$
$$+\frac{\sigma_T}{a}\left(|i\partial/\partial\lambda|^2 + |i\partial/\partial\rho|^2 + (3m_Q)^2(\vec{b}_\lambda^{\,2} + \vec{b}_\rho^{\,2})\right)$$

transverse oscillator plus longitudinal Laplacian

The non-factorizable part of the potential is

$$\tilde{V} = \frac{\vec{p}_1^{\,2} + m_Q^2}{x_1} + \frac{\vec{p}_2^{\,2} + m_Q^2}{x_2}$$
$$+ \frac{\vec{p}_3^{\,2} + m_Q^2}{x_3} - 3(\vec{p}_1^{\,2} + \vec{p}_2^{\,2} + \vec{p}_3^{\,2}) - 9m_Q^2$$

represented by a matrix calculated in the eigenstates of H0

Single-flavor baryons

have no “good diquark” correlations between quarks if tHooft-induced

of course, we not just have all masses , but all light-front wave functions as well! Can be used to calculate PDFs,FFs,GPDs

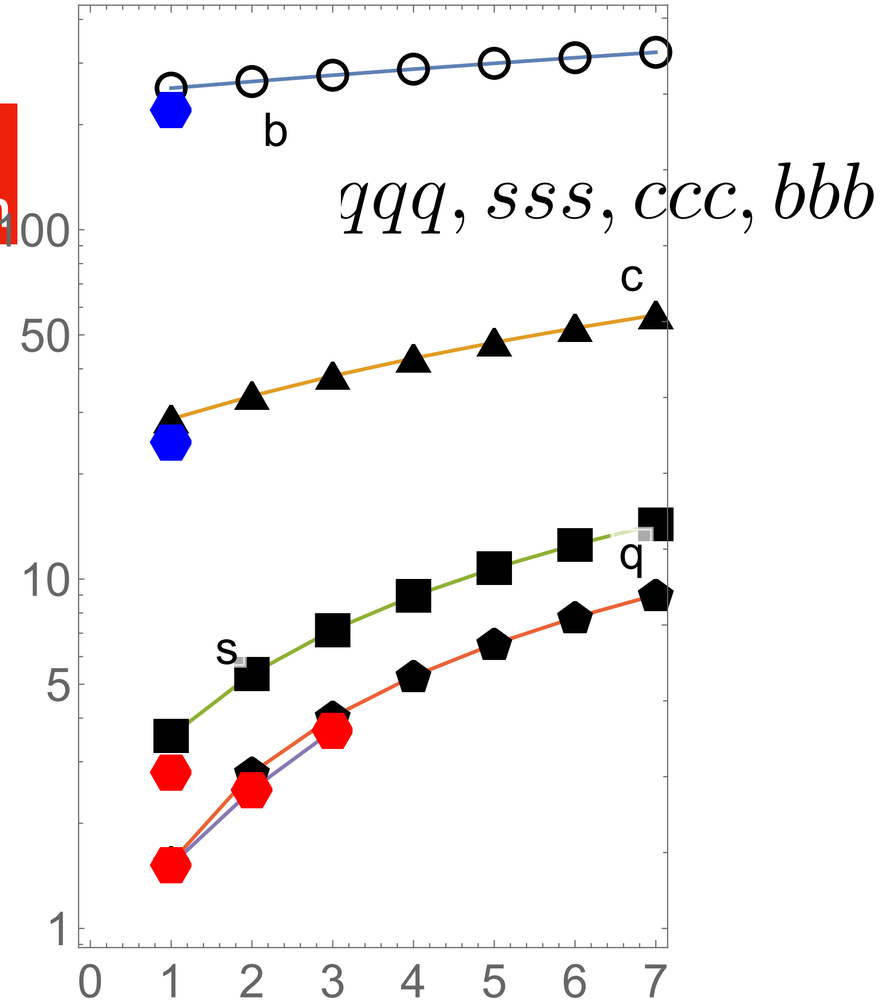

FIG. 9. Squared masses of baryons $M^2_{n+1}(Q, \frac{3}{2})$ in GeV^2, versus the principal quantum number $n+1 = 1..7$. The black circles, triangles, squared and pentagons are results of our calculations for the flavors b, c, s, q. The red hexagons are the experimental values of three Δ^{++} and one Ω^- masses, from PDG. The two blue hexagons are model predictions for masses of *ccc* and *bbb* baryons, from Table I

Hadronic structure on the light-front V. Diquarks, Nucleons and multiquark Fock components

e-Print: 2208.04428

phenomenology
scalar diquarks are deeply bound

assuming that the standard spin-spin interactions are of the form $(\vec{\sigma 1}\vec{\sigma 2})$,

this spin interaction can be eliminated

$$M(1{+}ud) - M(0{+}ud)\ (1) \approx$$

$$(2M(\Sigma{*}Q) + M(\Sigma Q)/3 - M(\Lambda Q) \approx 0.21\ \text{GeV}$$

diquarks are baryons in Nc=2 theory
which has Pauli-Gursey symmetry
so scalar diquark is degenerate with the pion
and vector degenerate with vector mesons

the instanton-induced ’t Hooft vertex.

$$\frac{G_{qq}}{G_{\bar{q}q}} = \frac{1}{N_c - 1}$$

so it is 1 for Nc=2 and 1/2 for Nc=3 and -1 in QED

Scalar diquarks become
Cooper pair in dense quark matter
=> color superconductors

DIQUARK PAIRING IN THE NUCLEONS

quasilocal approximation N versus Delta masses and WFs

$$H_{ud} = -G_{ud}\delta(\vec{r}_u - \vec{r}_d)$$

two diquark correlation channels in N (d with 2 u's) already makes noticeable differencesfor WFs especially near x->1

note that effect of pairing is smaller in excited states

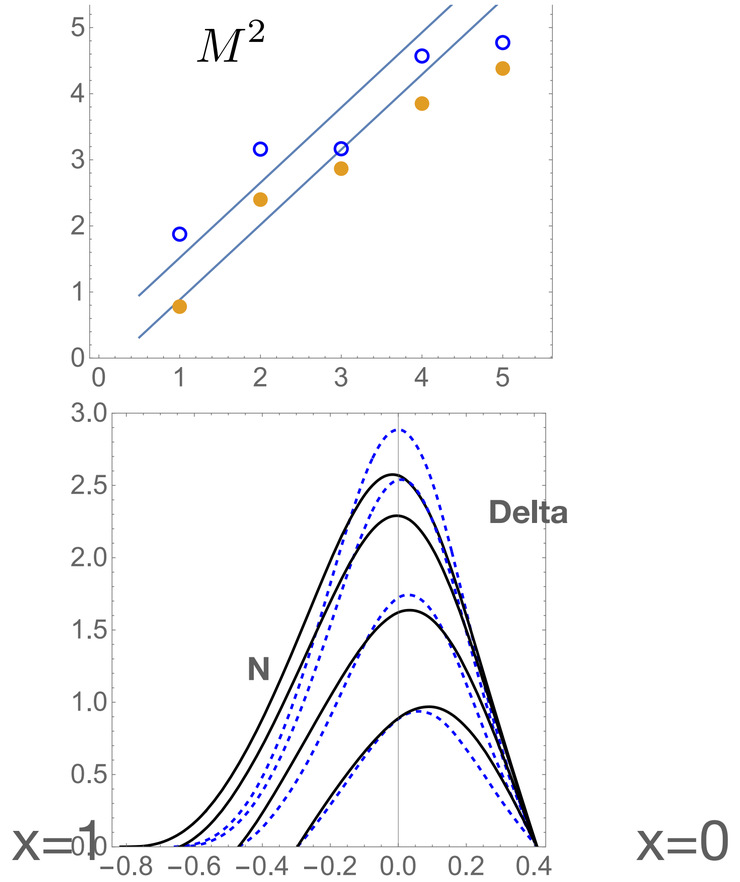

FIG. 6: Upper: Squared masses of the Delta (open points) and N (closed) resonances versus their successive quantum number n. The two straight lines shown for comparison, are the Regge trajectories fitted to the experimental values of $M^2(J)$, versus the total angular momentum J, with the slope $\alpha' = 0.88\,GeV^2$.
Lower: LFWFs for the lowest Delta (dashed lines) and N (solid lines). The plots are shown versus the Jacobi coordinate λ, for fixed $\rho = 0, 0.1, 0.2, 0.3$, top to bottom.

e-Print: 2208.04428

Nucleon and Delta Formfactors are approximately 1/Q^4

but show differences at large enough Q, Delta is softer which means its size is about 2^(1/4) times larger

$$F_1(t) = \int dx H(x,0,t)$$

N

$$A(t) = \int dx\, x H(x,0,t)$$

$$A(Q^2)/F_1(Q^2)$$

Delta

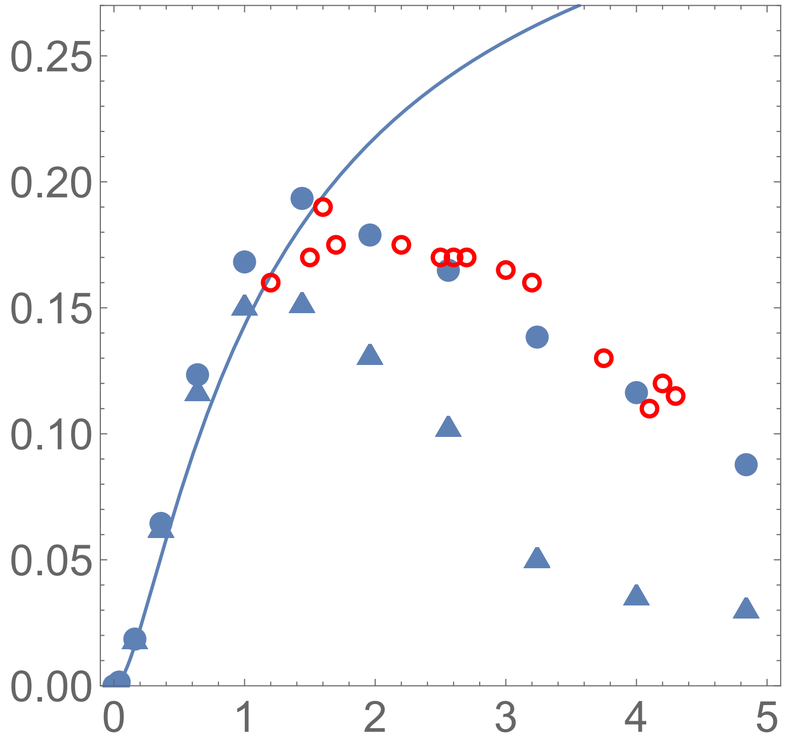

N

Delta

FIG. 8: $Q^4 F_1^d(Q^2)$, (GeV^4) versus the momentum transfer Q^2 (GeV^2). The triangles and closed points correspond to the Delta and Proton LFWFs, respectively. The red circles are extraction from the experimental data on the p and n formfactors mentioned in the text. The solid line shown for comparison, corresponds to the dipole form factor $Q^4/(1+Q^2/m_\rho^2)^2$.

paper VI # Nucleon and Delta GPDs

e-Print: 2301.12238

Zero skewness:

$$H(x,0,t) = \int_P \delta(x-x_1)\,\psi^{+*}([x_i', k_{i\perp}', \lambda_i])\psi^{+}([x_i, k_{i\perp}, \lambda_i])$$

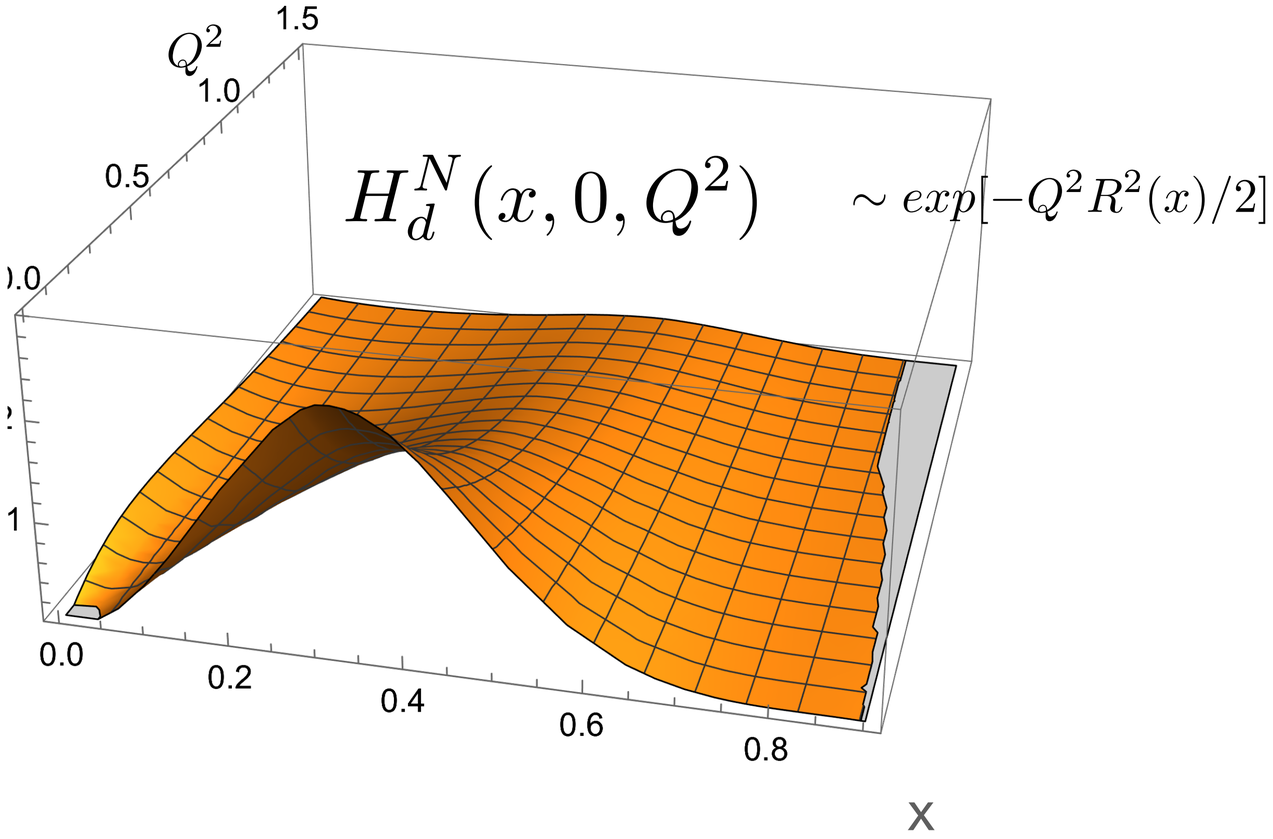

it is a formfactor but for particular x of the struck quark, and that turns out to be Gaussians, with x-dependent slopes

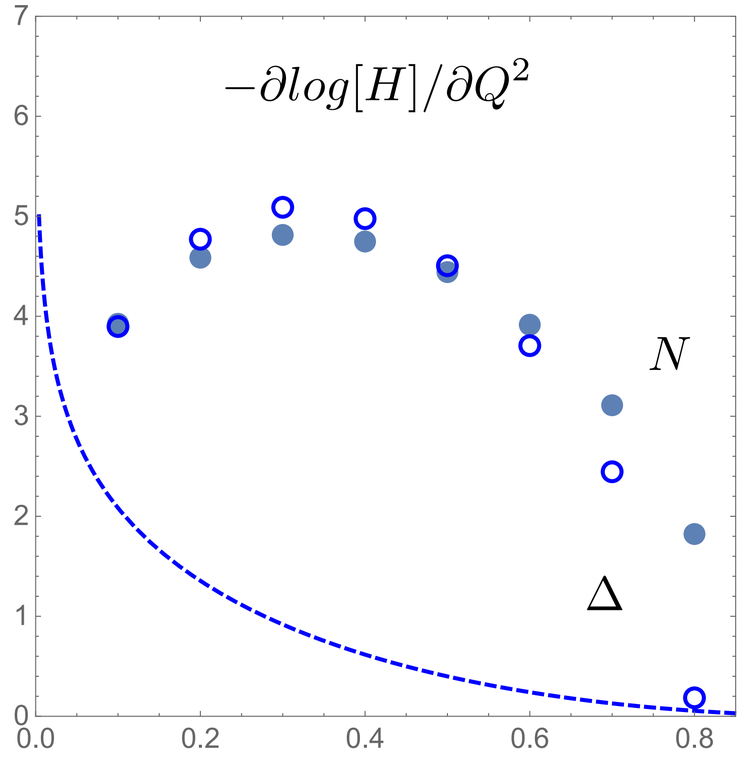

Revolution in hadronic spectroscopy -> multiquark hadrons

since 1960's they were considered "exotics" with questionable experimental support, but not anymore

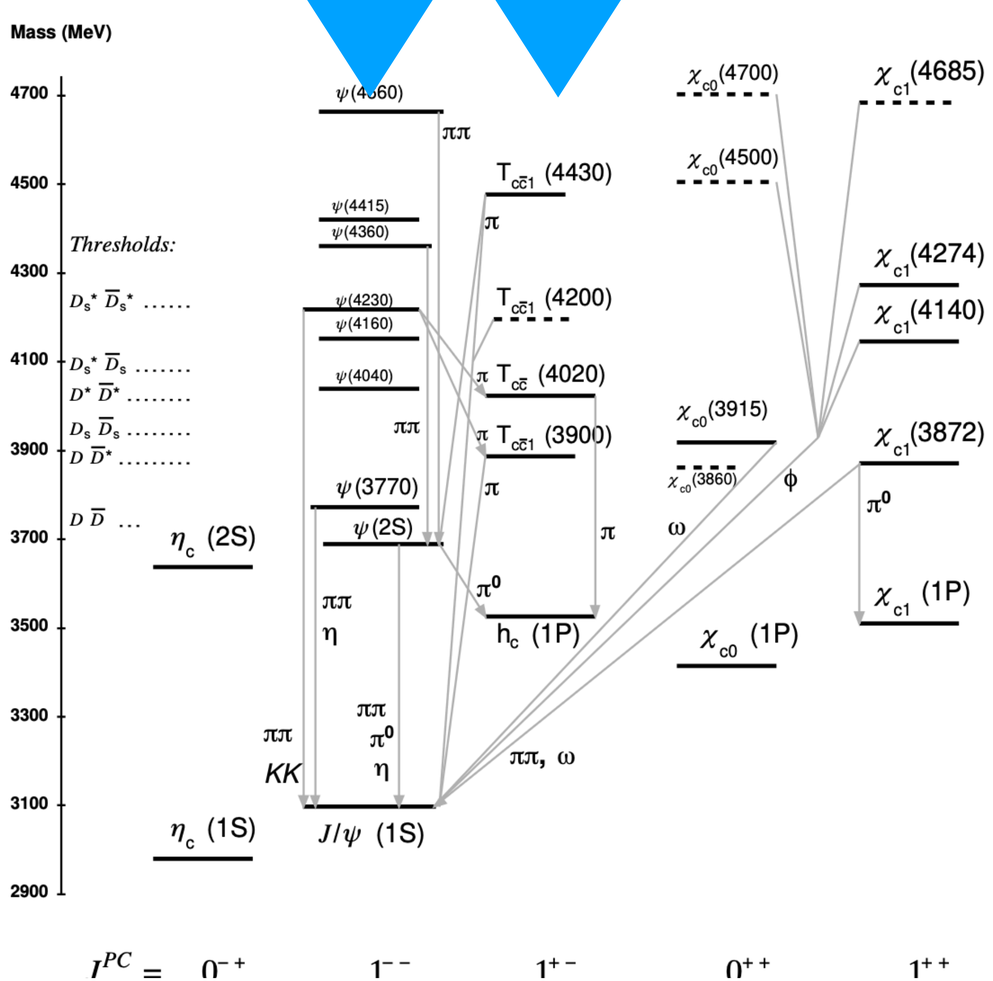

in axial 1^+- channel **4 tetras** and only one charmonium
in vector 1^— 9 psi's out of which only 5 charmonia
and also **4 tetras**

some of them are hybrids ccg

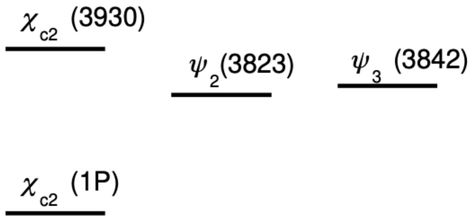

Tells us about adding quark pair as sigma and pion

$$\psi(R_9) = u(R_9)/R_9^4$$

$$\mathbf{H}=\left[\left(-\frac{d^2}{dR_9^2} + \frac{12}{R_9^2} \right) \frac{1}{2M} + (4M + V) \right] \mathbf{u}$$

2308.05638

$$M(2S) - M(1S) \approx 370\, MeV$$

$$M(3S) - M(1S) \approx 689\, MeV$$

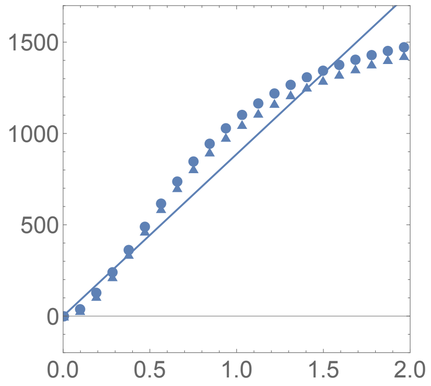

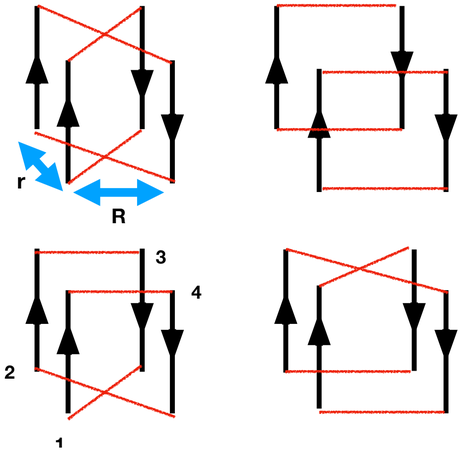

experiment (ATLAS)

$$M(2) - M(1) \approx 250\, MeV$$

$$M(3) - M(1) \approx 600\, MeV$$

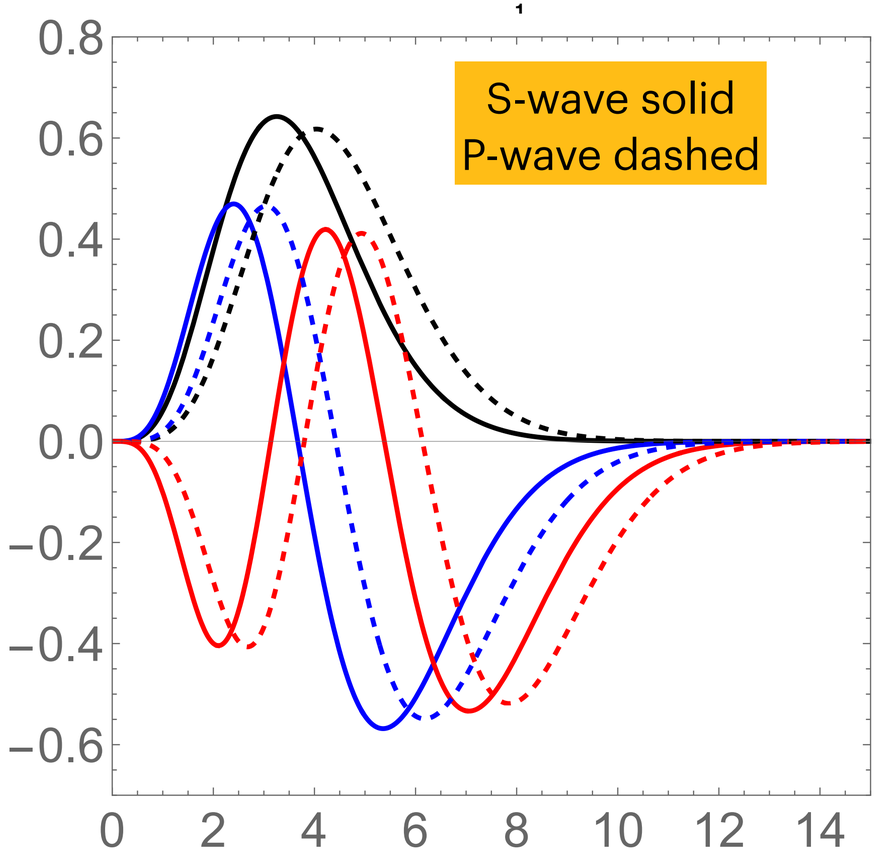

Novel technique to find multiquark states which obey Fermi statistics (started from P-shell and D-shell baryons)

[Miesch and Shuryak, 2024].

S-shell (L = 0) pentaquarks has color-spin-flavor dimension of ``monom'' space $36 \times 25 \times 25 = 746496$,

P-shell (L = 1) states. another factor of 4, in total O(10^6) monoms

:

At first sight, writing operators as matrices in such a large space may appear prohibitive, even with the aid of Mathematica. Fortunately, this is not the case, And how to enforce Fermi statistics?

We worked out representations of permutation groups S(n)
Procedure:
(1) find 2 generators of S_n group as explicit matrices,
(2)diagonalize those,
(3) find common eigenvectors of them with eigenvalues -1

Where pentaquarks become chaotic?

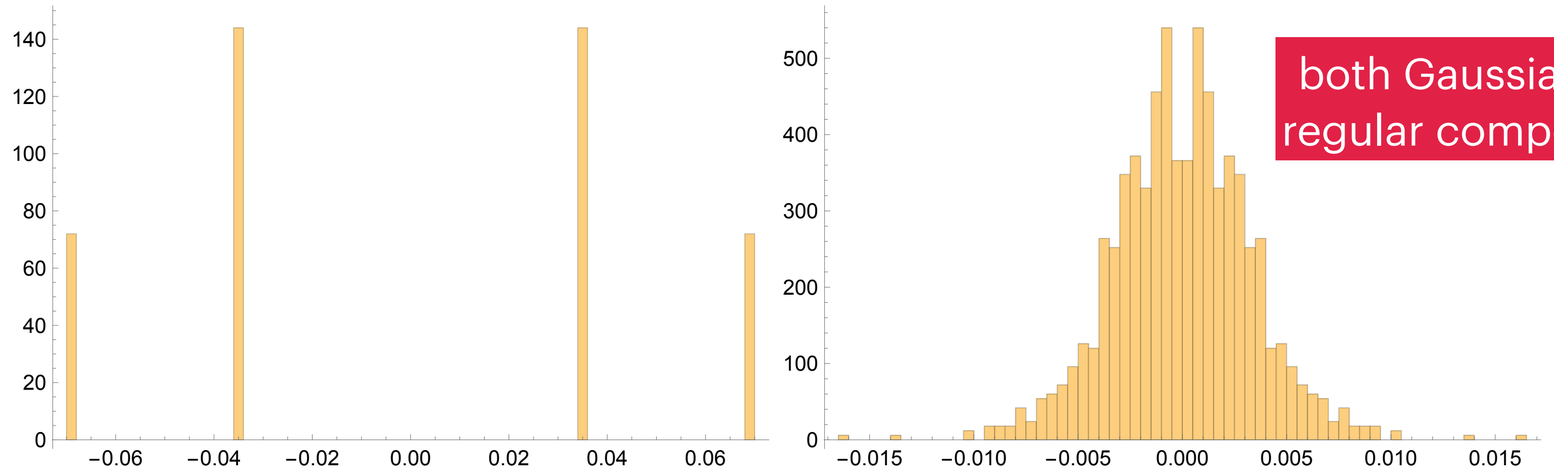

Fig. 9.3.2 Distribution of monom coefficients for an S-shell state with $L = 0$, $S = 5/2$, $I = 1/2$ (upper panel) and for a P-shell state with $L = 1$, $S = 1/2$, $I = 1/2$ (lower panel).

Quantum few-body systems are known to undergo a transition to the so-called quantum chaos regime

This phenomenon is well documented in atomic and nuclear systems with several particles or holes near closed shells. A historically important example is the cerium atom, which has four valence electrons and thus 12 effective coordinates.
even its lowest-energy states display chaotic behavior

T. Schäfer and E. V. Shuryak, Phys. Rev. Lett. **75**, 1707 (1995), arXiv:hep-ph/9410372.

instanton-induced effects in correlators, predicted R(0++)=0.2 fm

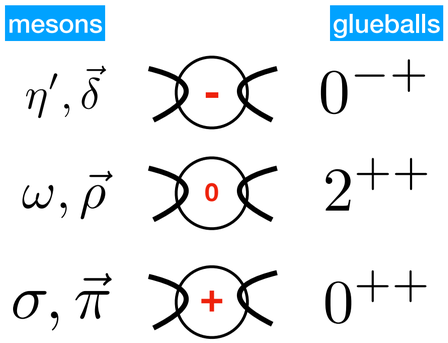

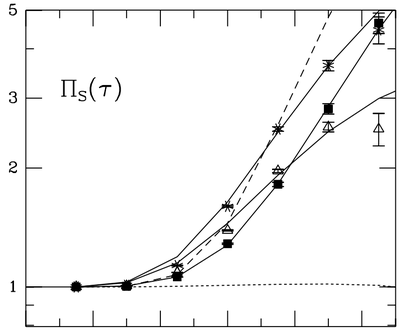

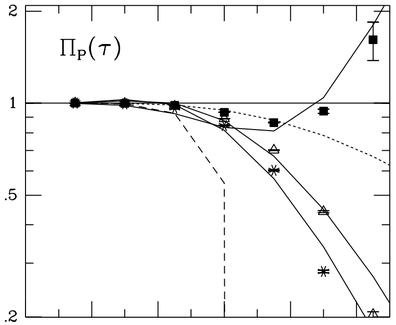

Glueballs, Constituent Gluons and Instantons

Edward Shuryak* and Ismail Zahed†

instead of short distances we look at excited states first and establish ``constituent gluon" model

H. B. Meyer and M. J. Teper, Nucl. Phys. B Proc. Suppl. **129**, 200 (2004), arXiv:hep-lat/0308035.

molecules and instanton

note size difference

T. Schäfer and E. V. Shuryak, Phys. Rev. Lett. **75**, 1707 (1995), arXiv:hep-ph/9410372.

instanton-induced effects in correlators, predicted R(0++)=0.2 fm

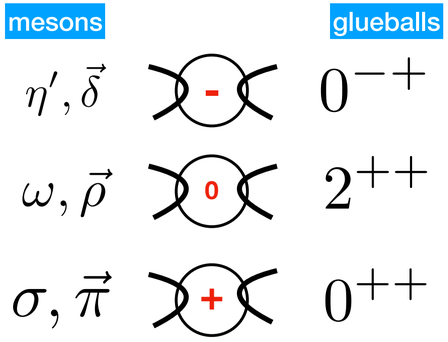

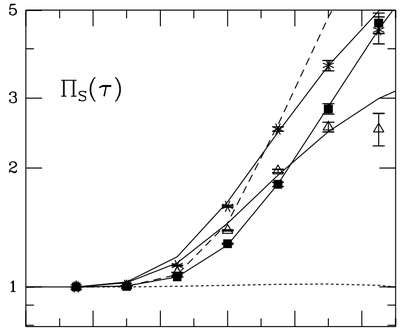

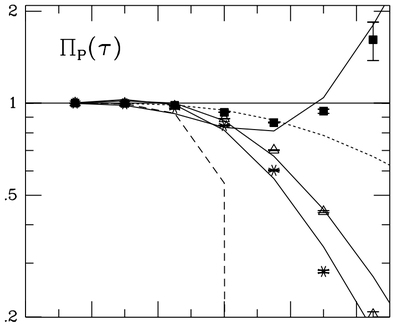

Glueballs, Constituent Gluons and Instantons

Edward Shuryak* and Ismail Zahed†

instead of short distances we look at excited states first and establish ``constituent gluon" model

H. B. Meyer and M. J. Teper, Nucl. Phys. B Proc. Suppl. **129**, 200 (2004), arXiv:hep-lat/0308035.

studies. The model parameters are chosen to reproduce the three higher states in the scalar channel, which, unlike the lowest $n = 0$ state, have "normal" hadronic sizes (see the table of r.m.s. radii) and are therefore less sensitive to short-distance forces. The most important parameter obtained in this way is the effective gluon mass, fitted to be

$$m_g = 0.90\,\mathrm{GeV}. \qquad (11)$$

molecules and instanton

note size difference

T. Schäfer and E. V. Shuryak, Phys. Rev. Lett. **75**, 1707 (1995), arXiv:hep-ph/9410372.

instanton-induced effects in correlators, predicted R(0++)=0.2 fm

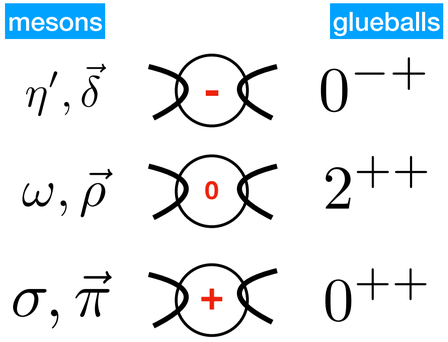

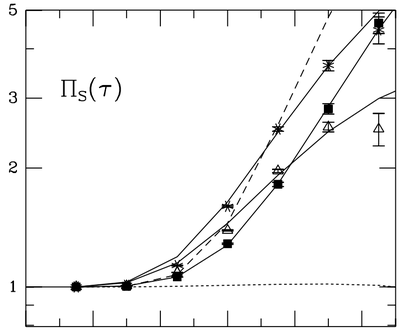

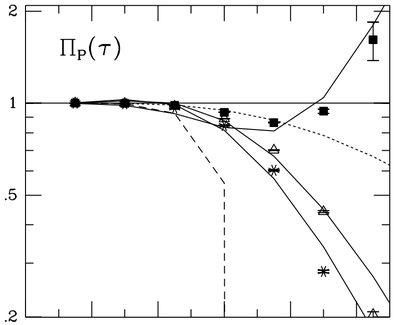

Glueballs, Constituent Gluons and Instantons

Edward Shuryak* and Ismail Zahed†

instead of short distances we look at excited states first and establish ``constituent gluon" model

H. B. Meyer and M. J. Teper, Nucl. Phys. B Proc. Suppl. **129**, 200 (2004), arXiv:hep-lat/0308035.

studies. The model parameters are chosen to reproduce the three higher states in the scalar channel, which, unlike the lowest $n = 0$ state, have "normal" hadronic sizes (see the table of r.m.s. radii) and are therefore less sensitive to short-distance forces. The most important parameter obtained in this way is the effective gluon mass, fitted to be

$$m_g = 0.90\,\mathrm{GeV}. \qquad (11)$$

non relativistic Schrodinger eqn used with instanton-induced potentials V®

molecules and instanton

note size difference

T. Schäfer and E. V. Shuryak, Phys. Rev. Lett. **75**, 1707 (1995), arXiv:hep-ph/9410372.

instanton-induced effects in correlators, predicted R(0++)=0.2 fm

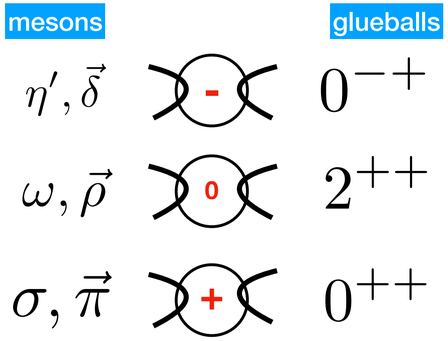

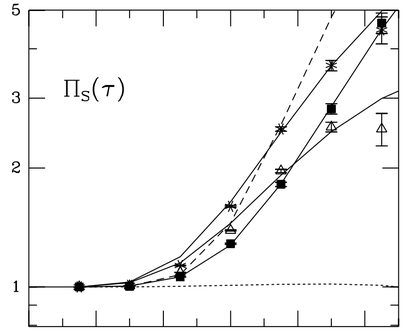

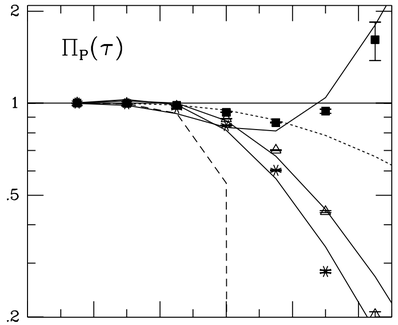

Glueballs, Constituent Gluons and Instantons

Edward Shuryak* and Ismail Zahed†

instead of short distances we look at excited states first and establish ``constituent gluon" model

H. B. Meyer and M. J. Teper, Nucl. Phys. B Proc. Suppl. **129**, 200 (2004), arXiv:hep-lat/0308035.

studies. The model parameters are chosen to reproduce the three higher states in the scalar channel, which, unlike the lowest $n = 0$ state, have "normal" hadronic sizes (see the table of r.m.s. radii) and are therefore less sensitive to short-distance forces. The most important parameter obtained in this way is the effective gluon mass, fitted to be

$$m_g = 0.90\,\mathrm{GeV}. \qquad (11)$$

non relativistic Schrodinger eqn used with instanton-induced potentials V®

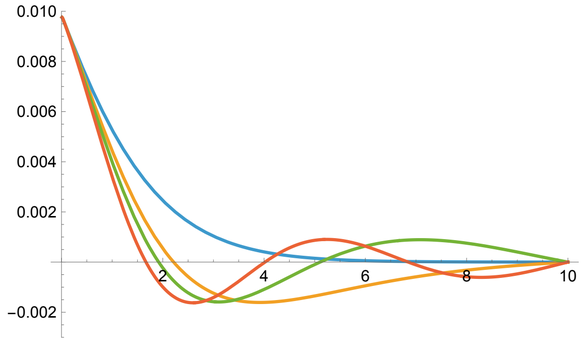

note size difference

molecules and instanton

T. Schäfer and E. V. Shuryak, Phys. Rev. Lett. **75**, 1707 (1995), arXiv:hep-ph/9410372.

instanton-induced effects in correlators, predicted R(0++)=0.2 fm

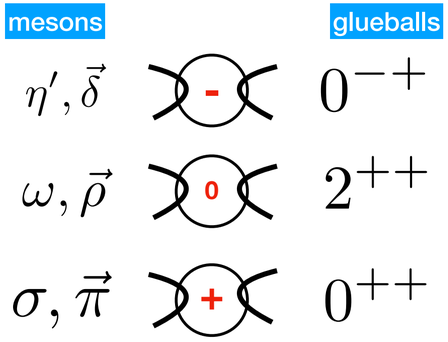

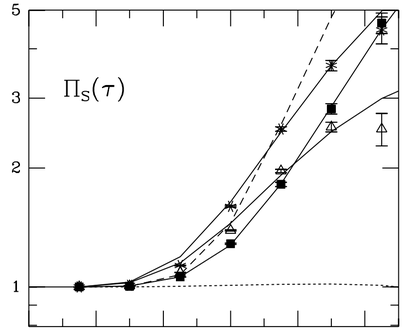

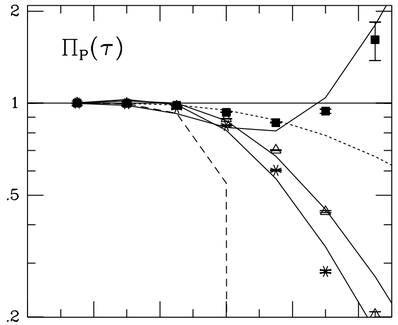

Glueballs, Constituent Gluons and Instantons

Edward Shuryak* and Ismail Zahed†

instead of short distances we look at excited states first and establish ``constituent gluon" model

H. B. Meyer and M. J. Teper, Nucl. Phys. B Proc. Suppl. **129**, 200 (2004), arXiv:hep-lat/0308035.

studies. The model parameters are chosen to reproduce the three higher states in the scalar channel, which, unlike the lowest $n = 0$ state, have "normal" hadronic sizes (see the table of r.m.s. radii) and are therefore less sensitive to short-distance forces. The most important parameter obtained in this way is the effective gluon mass, fitted to be

$$m_g = 0.90\,\mathrm{GeV}. \qquad (11)$$

non relativistic Schrodinger eqn used with instanton-induced potentials V®

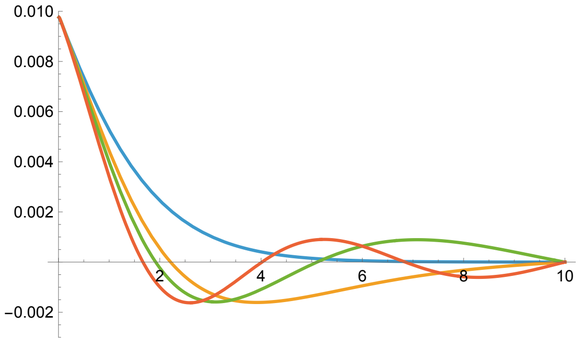

note size difference

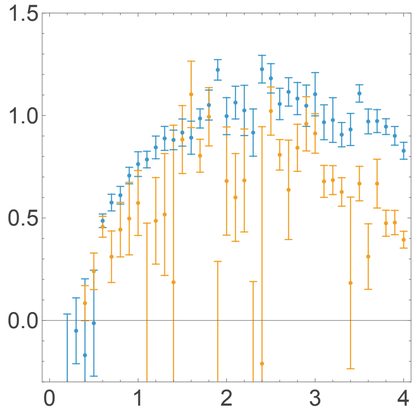

molecules and instanton

T. Schäfer and E. V. Shuryak, Phys. Rev. Lett. **75**, 1707 (1995), arXiv:hep-ph/9410372.

instanton-induced effects in correlators, predicted R(0++)=0.2 fm

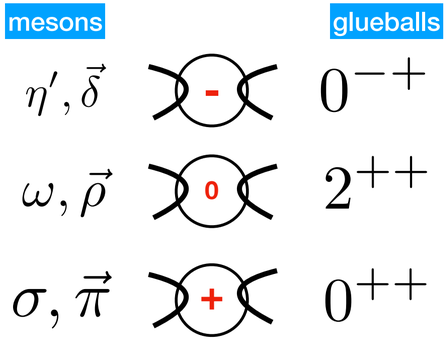

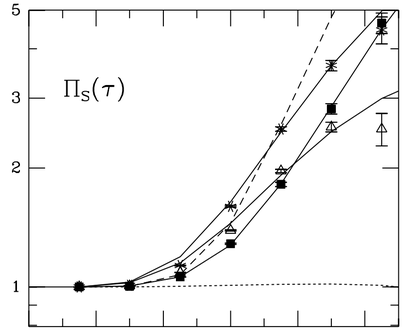

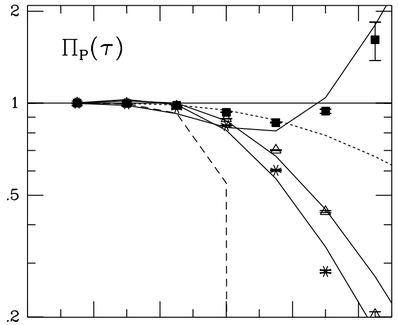

Glueballs, Constituent Gluons and Instantons

Edward Shuryak* and Ismail Zahed†

instead of short distances we look at excited states first and establish ``constituent gluon" model

studies. The model parameters are chosen to reproduce the three higher states in the scalar channel, which, unlike the lowest $n = 0$ state, have "normal" hadronic sizes (see the table of r.m.s. radii) and are therefore less sensitive to short-distance forces. The most important parameter obtained in this way is the effective gluon mass, fitted to be

$$m_g = 0.90\,\mathrm{GeV}. \qquad (11)$$

non relativistic Schrodinger eqn used with instanton-induced potentials V®

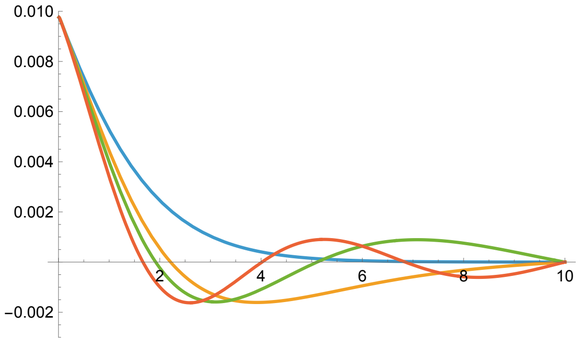

note size difference

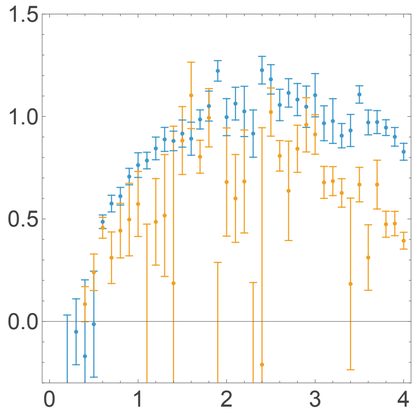

H. B. Meyer and M. J. Teper, Nucl. Phys. B Proc. Suppl. **129**, 200 (2004), arXiv:hep-lat/0308035.

J^{PC}	This work	Lattice [1, 23]
0^{++}	1.92 (BS: 1.4–1.5)	1.475(30)(65)
0^{++}	2.79	2.755(70)(120)
0^{++}	3.29	3.370(100)(150)
0^{++}	4.00	3.990(210)(180)
2^{++}	3.01	2.150(30)(100)
2^{++}	3.46	2.880(100)(130)
2^{++}	4.16	3.385(90)(150)
2^{++}	5.10	–
4^{++}	3.52	3.640(90)(160)
4^{++}	4.18	–
4^{++}	5.10	–
4^{++}	6.24	–
6^{++}	4.06	4.360(260)(200)
6^{++}	4.97	–
6^{++}	6.11	–
6^{++}	7.49	–
0^{-+}	2.65	2.250(60)(100)
0^{-+}	3.13	3.370(150)(150)
1^{+-}	–	2.94(17)
1^{--}	–	3.81(27)
3^{++}	–	3.38(15)
3^{+-}	–	3.70(23)
3^{--}	–	4.03(25)

molecules and instanton

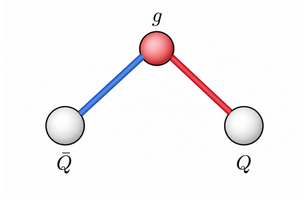

FIG. 1. Schematic setting of the variational calculation: heavy quarks $\bar{Q}$ and Q are static, and a "constituent gluon" g dynamical, connected to both by a linear potential.

obtained is shown in Fig.2(upper). Modern versions of this potentials from lattice studies are shown in Fig.2(lower).

Now we present details of the calculation. The

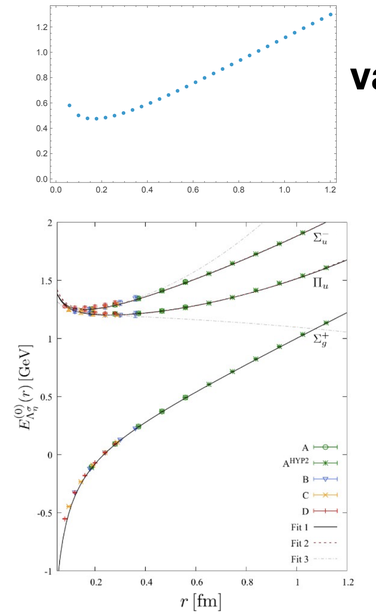

variational

lattice

FIG. 2. (Upper) Result of our variational calculation of $\Sigma_u^-(r)$ potential versus quark-antiquark separation $r,(fm)$.(Lower) The lowest hybrid static BO energies Π_u and Σ_u^- and the quarkonium static energy Σ_g^+, from lattice measurements reported in [8].

Hybrid hadrons at rest and on the light front

Edward Shuryak* and Ismail Zahed†

multiple non-charmonium states, tetraquarks or hybrids?

Before going into technical details, let us discuss simple qualitative estimates for the masses of tetraquarks and hybrid states. We begin by proposing a crude relation between meson and glueball masses. The constituent quark mass is about $M_q \approx 350\,\mathrm{MeV}$, while the constituent gluon mass, fitted from glueball spectra [1, 2], is $M_g \approx 900\,\mathrm{MeV}$. Their ratio ($\approx 2.57$) is close to the Casimir scaling ratio 9/4, which governs the strength of perturbative Coulomb interactions. The adjoint confining potential is also stronger by approximately the same factor [1, 2]. This suggests that Casimir scaling may be approximately used for glueball-to-meson mass ratios as well.

data

Proceeding further, the mass difference between hybrids and tetraquarks should include the difference between effective gluon mass and twice the effective quark mass. Assuming Casimir scaling, one estimates

$$M_g - 2M_q \approx M_g/4 \approx 225\,\mathrm{MeV}.$$

This combination should therefore appear in the difference between hybrid and tetraquark masses:

$$M(\mathrm{hybrids}) - M(\mathrm{tetras}) \approx M_g - 2M_q \sim 200\,\mathrm{MeV}. \quad (1)$$

similar potentials lead to similar WFs

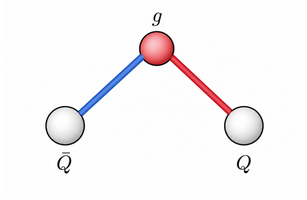

FIG. 1. Schematic setting of the variational calculation: heavy quarks $\bar{Q}$ and Q are static, and a "constituent gluon" g dynamical, connected to both by a linear potential.

obtained is shown in Fig.2(upper). Modern versions of this potentials from lattice studies are shown in Fig.2(lower).

Now we present details of the calculation. The

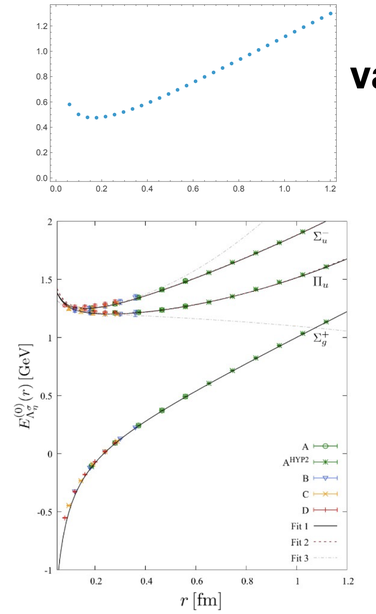

variational

lattice

FIG. 2. (Upper) Result of our variational calculation of $\Sigma_u^-(r)$ potential versus quark-antiquark separation $r, (fm)$.(Lower) The lowest hybrid static BO energies Π_u and Σ_u^- and the quarkonium static energy Σ_g^+, from lattice measurements reported in [8].

Hybrid hadrons at rest and on the light front

Edward Shuryak* and Ismail Zahed†

multiple non-charmonium states, tetraquarks or hybrids?

Before going into technical details, let us discuss simple qualitative estimates for the masses of tetraquarks and hybrid states. We begin by proposing a crude relation between meson and glueball masses. The constituent quark mass is about $M_q \approx 350\,\mathrm{MeV}$, while the constituent gluon mass, fitted from glueball spectra [1, 2], is $M_g \approx 900\,\mathrm{MeV}$. Their ratio ($\approx 2.57$) is close to the Casimir scaling ratio $9/4$, which governs the strength of perturbative Coulomb interactions. The adjoint confining potential is also stronger by approximately the same factor [1, 2]. This suggests that Casimir scaling may be approximately used for glueball-to-meson mass ratios as well.

Proceeding further, the mass difference between hybrids and tetraquarks should include the difference between effective gluon mass and twice the effective quark mass. Assuming Casimir scaling, one estimates

$$M_g - 2M_q \approx M_g/4 \approx 225\,\mathrm{MeV}.$$

This combination should therefore appear in the difference between hybrid and tetraquark masses:

$$M(\mathrm{hybrids}) - M(\mathrm{tetras}) \approx M_g - 2M_q \sim 200\,\mathrm{MeV}.$$

We have solved Schrodinger equation for Σ_g^- hybrids and compare their energies to charmonium Σ_g^+, using parameterizations of potentials shown in lower Fig.2. The first three levels are $((GeV))$

$$E_{\Sigma_g^-}[n]/GeV = 4.46, 4.96, 5.42, ... \qquad (31)$$

The first two we relate to two experimentally observed states (all in MeV)

$$\begin{aligned} \psi(4360), M &= 4374 \pm 7\,, \Gamma = 118 \pm 12 \\ \psi(4660), M &= 4630 \pm 6\,, \Gamma = 72 \pm 13 \end{aligned} \qquad (32)$$

data

due to their decay pattern (see below) .

Note that we only use spin-independent potential, and that charmonia levels in the same approximation are

$$E_{\gamma+}[n]/GeV = 3.10.\, 3.67.\, 4.09... \qquad (33)$$

similar potentials lead to similar WFs

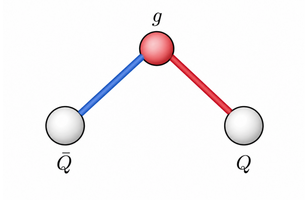

FIG. 1. Schematic setting of the variational calculation: heavy quarks $\bar{Q}$ and Q are static, and a "constituent gluon" g dynamical, connected to both by a linear potential.

obtained is shown in Fig.2(upper). Modern versions of this potentials from lattice studies are shown in Fig.2(lower).

Now we present details of the calculation. The

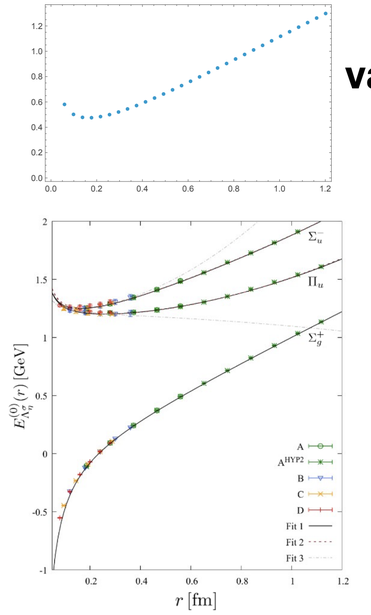

FIG. 2. (Upper) Result of our variational calculation of $\Sigma_u^-(r)$ potential versus quark-antiquark separation $r,(fm)$.(Lower) The lowest hybrid static BO energies Π_u and Σ_u^- and the quarkonium static energy Σ_g^+, from lattice measurements reported in [8].

Hybrid hadrons at rest and on the light front

Edward Shuryak* and Ismail Zahed†

multiple non-charmonium states, tetraquarks or hybrids?

Before going into technical details, let us discuss simple qualitative estimates for the masses of tetraquarks and hybrid states. We begin by proposing a crude relation between meson and glueball masses. The constituent quark mass is about $M_q \approx 350\,\mathrm{MeV}$, while the constituent gluon mass, fitted from glueball spectra [1, 2], is $M_g \approx 900\,\mathrm{MeV}$. Their ratio ($\approx 2.57$) is close to the Casimir scaling ratio $9/4$, which governs the strength of perturbative Coulomb interactions. The adjoint confining potential is also stronger by approximately the same factor [1, 2]. This suggests that Casimir scaling may be approximately used for glueball-to-meson mass ratios as well.

Proceeding further, the mass difference between hybrids and tetraquarks should include the difference between effective gluon mass and twice the effective quark mass. Assuming Casimir scaling, one estimates

$$M_g - 2M_q \approx M_g/4 \approx 225\,\mathrm{MeV}.$$

This combination should therefore appear in the difference between hybrid and tetraquark masses:

$$M(\mathrm{hybrids}) - M(\mathrm{tetras}) \approx M_g - 2M_q \sim 200\,\mathrm{MeV}.$$

We have solved Schrodinger equation for Σ_g^- hybrids and compare their energies to charmonium Σ_g^+, using parameterizations of potentials shown in lower Fig.2. The first three levels are $((GeV))$

$$E_{\Sigma_g^-}[n]/GeV = 4.46, 4.96, 5.42, ... \qquad (31)$$

The first two we relate to two experimentally observed states (all in MeV)

$$\begin{aligned} \psi(4360), M &= 4374 \pm 7\,, \Gamma = 118 \pm 12 \\ \psi(4660), M &= 4630 \pm 6\,, \Gamma = 72 \pm 13 \end{aligned} \qquad (32)$$

data

due to their decay pattern (see below) .

Note that we only use spin-independent potential, and that charmonia levels in the same approximation are

$$E_{\Sigma_g^+}[n]/GeV = 3.10, 3.67, 4.09... \qquad (33)$$

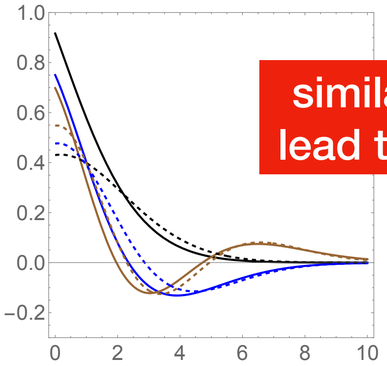

FIG. 3. Three lowest normalized wave functions (black,blue and brown) versus $r(GeV^{-1})$for Σ_g^+ charmonia (solid lines) compared to those for three lowest hybrids (dashed lines of the same colors).

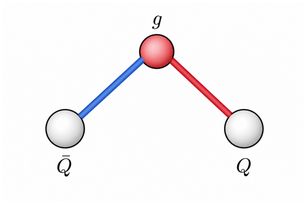

FIG. 1. Schematic setting of the variational calculation: heavy quarks $\bar{Q}$ and Q are static, and a "constituent gluon" g dynamical, connected to both by a linear potential.

obtained is shown in Fig.2(upper). Modern versions of this potentials from lattice studies are shown in Fig.2(lower).

Now we present details of the calculation. The

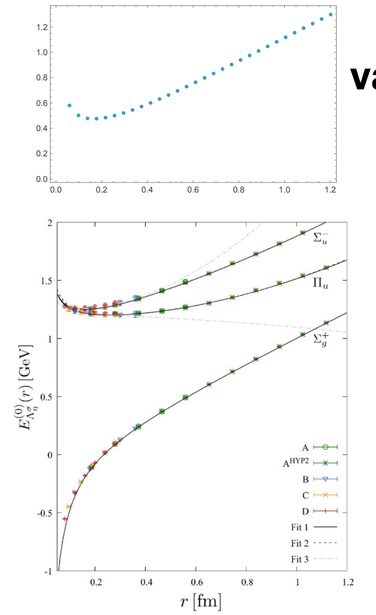

FIG. 2. (Upper) Result of our variational calculation of $\Sigma_u^-(r)$ potential versus quark-antiquark separation $r,(fm)$.(Lower) The lowest hybrid static BO energies Π_u and Σ_u^- and the quarkonium static energy Σ_g^+, from lattice measurements reported in [8].

Hybrid hadrons at rest and on the light front

Edward Shuryak* and Ismail Zahed†

multiple non-charmonium states, tetraquarks or hybrids?

Before going into technical details, let us discuss simple qualitative estimates for the masses of tetraquarks and hybrid states. We begin by proposing a crude relation between meson and glueball masses. The constituent quark mass is about $M_q \approx 350\,\mathrm{MeV}$, while the constituent gluon mass, fitted from glueball spectra [1, 2], is $M_g \approx 900\,\mathrm{MeV}$. Their ratio ($\approx 2.57$) is close to the Casimir scaling ratio 9/4, which governs the strength of perturbative Coulomb interactions. The adjoint confining potential is also stronger by approximately the same factor [1, 2]. This suggests that Casimir scaling may be approximately used for glueball-to-meson mass ratios as well.

Proceeding further, the mass difference between hybrids and tetraquarks should include the difference between effective gluon mass and twice the effective quark mass. Assuming Casimir scaling, one estimates

$$M_g - 2M_q \approx M_g/4 \approx 225\,\mathrm{MeV}.$$

This combination should therefore appear in the difference between hybrid and tetraquark masses:

$$M(\mathrm{hybrids}) - M(\mathrm{tetras}) \approx M_g - 2M_q \sim 200\,\mathrm{MeV}. \quad (1)$$

We have solved Schrodinger equation for Σ_g^- hybrids and compare their energies to charmonium Σ_g^+, using parameterizations of potentials shown in lower Fig.2. The first three levels are $((GeV))$

$$E_{\Sigma_g^-}[n]/GeV = 4.46, 4.96, 5.42, ... \quad (31)$$

The first two we relate to two experimentally observed states (all in MeV)

$$\begin{aligned} \psi(4360), M &= 4374 \pm 7\,, \Gamma = 118 \pm 12 \\ \psi(4660), M &= 4630 \pm 6\,, \Gamma = 72 \pm 13 \end{aligned} \quad (32)$$

data

due to their decay pattern (see below) .

Note that we only use spin-independent potential, and that charmonia levels in the same approximation are

$$E_{\sigma_+}[n]/GeV = 3.10, 3.67, 4.09... \quad (33)$$

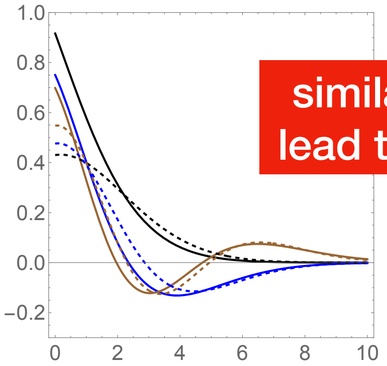

similar potentials lead to similar WFs

FIG. 3. Three lowest normalized wave functions (black,blue and brown) versus $r(GeV^{-1})$for Σ_g^+ charmonia (solid lines) compared to those for three lowest hybrids (dashed lines of the same colors).

$$\begin{vmatrix} 0.962506 & 0.221047 & 0.115586 \\ 0.248419 & 0.950676 & 0.126904 \\ 0.0890036 & 0.164056 & 0.972669 \end{vmatrix}$$

TABLE I. Overlaps defined in (35).

Hybrids on the LF, ccg and qqqg

forward WF on a triangle

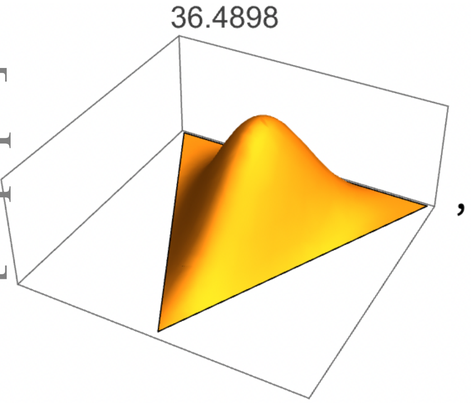

$$x_1 = \frac{2+\sqrt{6}\,\lambda+3\sqrt{2}\,\rho}{6},$$
$$x_2 = \frac{2+\sqrt{6}\,\lambda-3\sqrt{2}\,\rho}{6},$$
$$x_3 = \frac{1-\sqrt{6}\,\lambda}{3}.$$

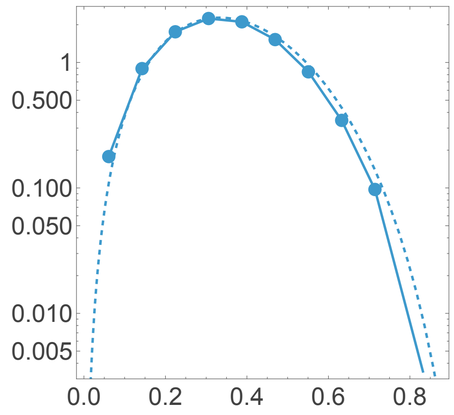

FIG. 6. Gluon PDF in the *ccg* hybrid, compared to the approximation $\sim x^3(1-x)^6$ (dashed line).

BARYON-GLUON $qqqg$ HYBRID ON THE LF

since here g is the heaviest it is in the center and identified with color junction

$$\alpha = -x_1 + x_2,$$
$$\beta = \frac{M_1 x_1 + M_2 x_2}{M_1+M_2} - x_3,$$
$$\gamma = \frac{M_1 x_1 + M_2 x_2 + M_3 x_3}{M_1+M_2+M_3} - x_4,$$
$$\delta = \frac{M_1 x_1 + M_2 x_2 + M_3 x_3 + M_4 x_4}{M_1+M_2+M_3+M_4}.$$

defined on 3d tetrahedron in 4d

$$\hat{H}_{\parallel}(a) = \sum_{i=1}^{3} \frac{\omega_q}{x_i} + \frac{\omega_g}{x_g} + \sigma_{qg}\left(3a + \frac{1}{a}\sum_{i=1}^{3}\left| i\frac{\partial}{\partial x_i} - i\frac{\partial}{\partial x_g}\right|^2\right),$$

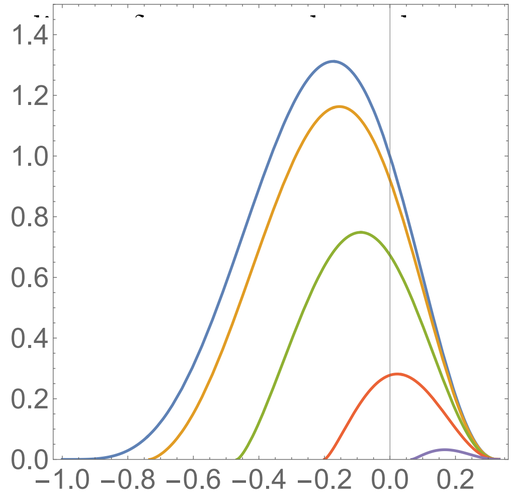

FIG. 7. Variational wave function as a function of γ, at $\alpha = 0$. Subseqquent curves, top to bottom, at $\beta = 0, 0.1, 0.2, 0.3, 0.4, 0.5$.

gluon PDF calculated to be

$$q(x) \propto x^{2.731956}(1-x)^{12.474919}.$$

to be related to exps. but first DGLAP needs to be modified at mu=1 GeV since m_g=0.9 GeV

Topological landscape of gauge fields

Chern-Simons number,

$$N_{CS} \equiv \frac{\epsilon^{\alpha\beta\gamma}}{16\pi^2} \int d^3x \left(A^a_\alpha \partial_\beta A^a_\gamma + \frac{1}{3}\epsilon^{abc} A^a_\alpha A^b_\beta A^c_\gamma \right),$$

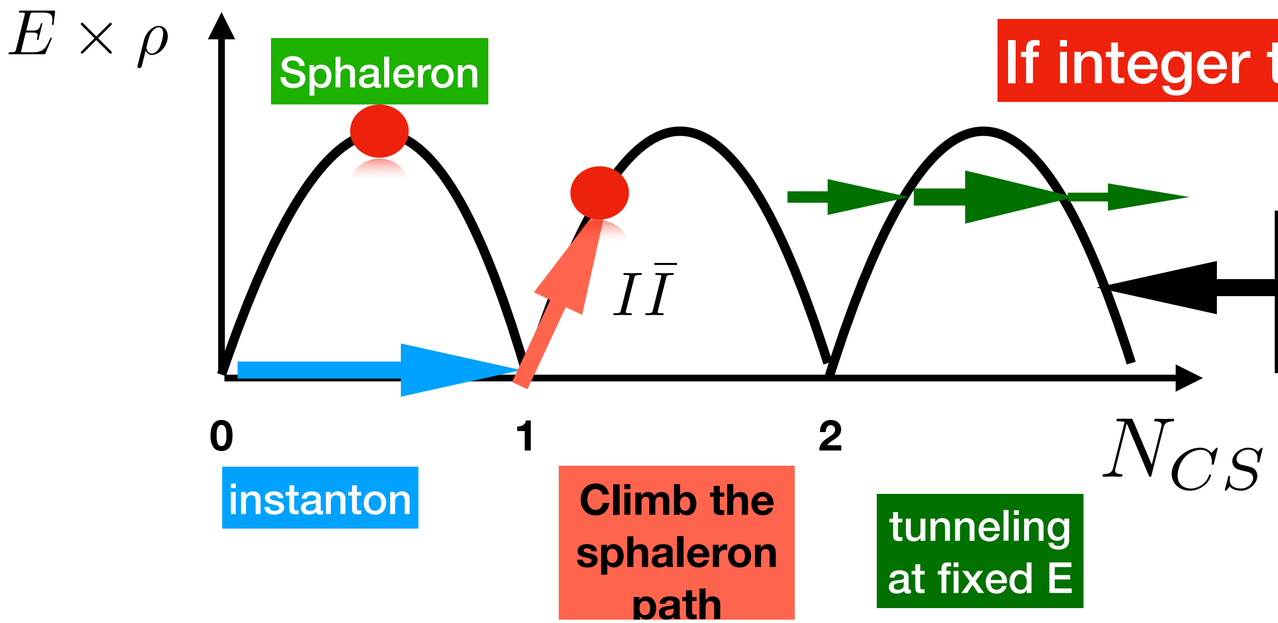

If integer then A is pure gauge, Gmunu=0

Sphaleron path, streamline or thimble

lines in parametric form

$$U_{\min}(k,\rho) = (1-k^2)^2 \frac{3\pi^2}{g^2\rho},$$

$$N_{CS}(k) = \frac{1}{4}\mathrm{sign}(k)(1-|k|)^2(2+|k|).$$

Conditional energy minimization Ostrovsky and Shuryak,2002)

instanton liquid model (ILM) has two components

$$\rho = 1/3\, fm, R = 1\, fm$$

$$\kappa = \pi^2 (\frac{\rho}{R})^4 \approx 0.12$$ ES, 1982

dilute:
consists of well-separated instantons
their collectivised zero modes = quark condensate

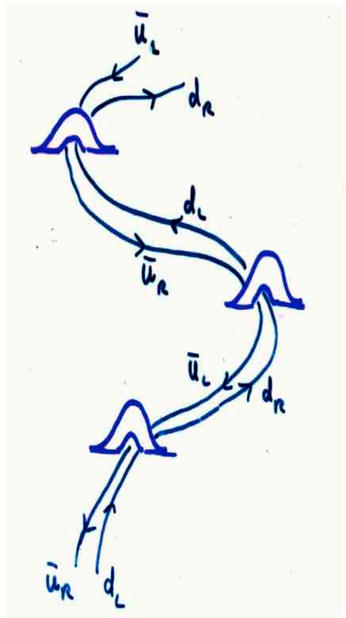

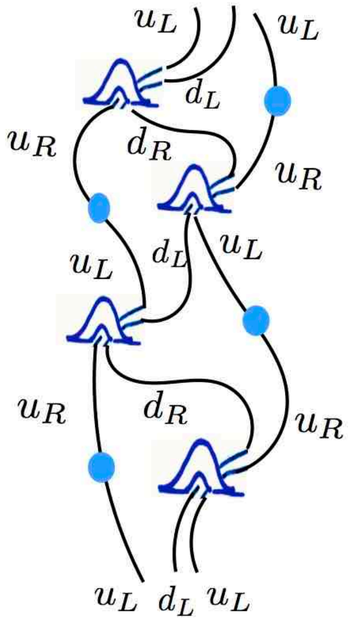

instanton liquid model (ILM) has two components

$$\rho = 1/3\, fm, R = 1\, fm$$

$$\kappa = \pi^2 (\frac{\rho}{R})^4 \approx 0.12$$ ES, 1982

dilute:
consists of well-separated
instantons
their collectivised zero
modes = quark condensate

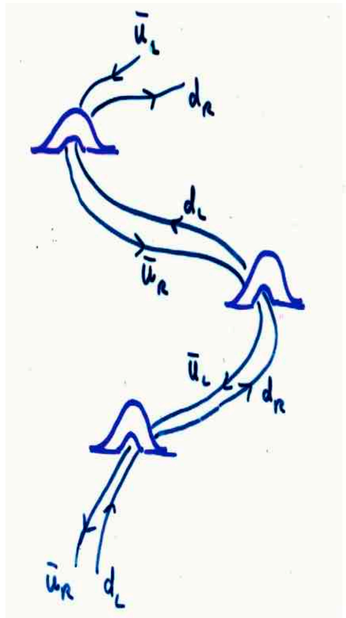

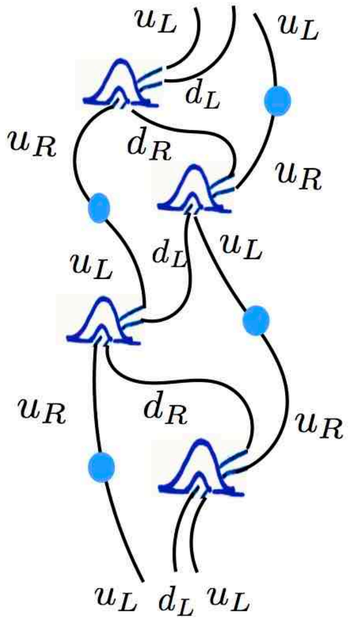

"molecular component"
which is denser
because overlapping
I and bar-I
has smaller action
but without near-zero
Dirac eigenvalues!

instanton liquid model (ILM) has two components

$$\rho = 1/3\, fm, R = 1\, fm$$

$$\kappa = \pi^2 (\frac{\rho}{R})^4 \approx 0.12$$ ES, 1982

dilute:
consists of well-separated
instantons
their collectivised zero
modes = quark condensate

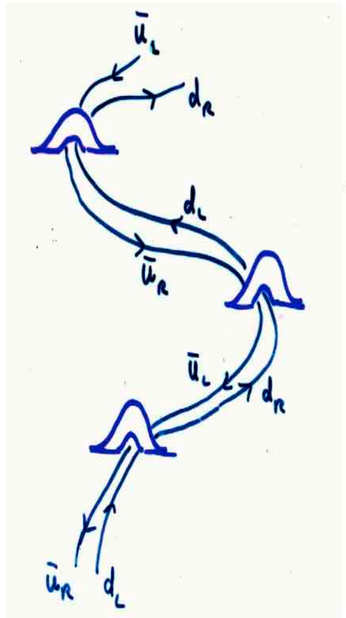

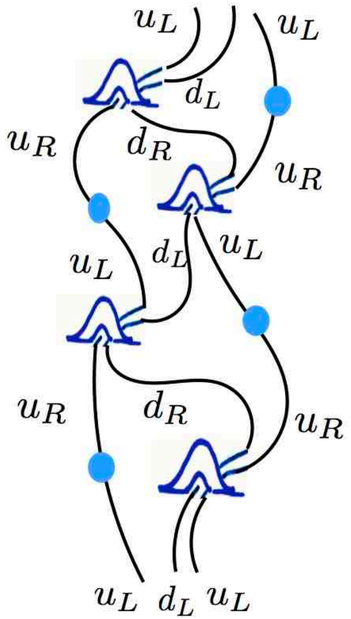

"molecular component"
which is denser
because overlapping
I and bar-I
has smaller action
but without near-zero
Dirac eigenvalues!

Ilgenfritz,ES 1988,1993

instanton liquid model (ILM) has two components

$$\rho = 1/3\, fm, R = 1\, fm$$

$$\kappa = \pi^2 (\frac{\rho}{R})^4 \approx 0.12$$ ES, 1982

dilute:
consists of well-separated
instantons
their collectivised zero
modes = quark condensate

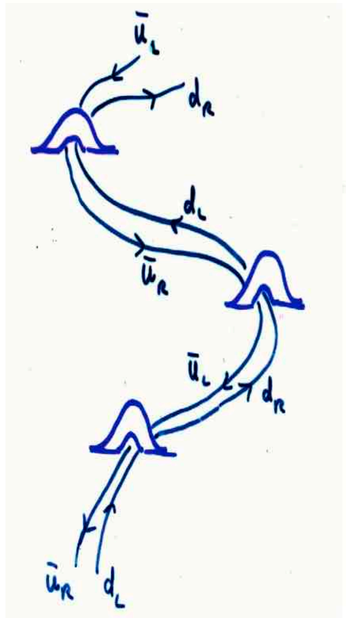

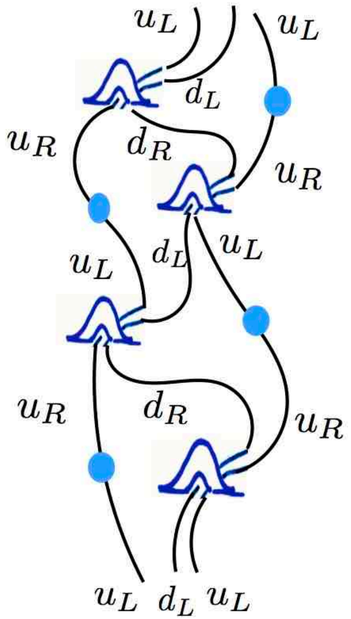

"molecular component"
which is denser
because overlapping
I and bar-I
has smaller action
but without near-zero
Dirac eigenvalues!

Ilgenfritz,ES 1988,1993

current lattice studies with G^2,G^3 observables
and gradient flow cooling (extrapolated to zero time)
suggest kappa=O(1)

instanton liquid model (ILM) has two components

$$\rho = 1/3\, fm, R = 1\, fm$$

$$\kappa = \pi^2 (\frac{\rho}{R})^4 \approx 0.12$$ ES, 1982

dilute:
consists of well-separated instantons
their collectivised zero modes = quark condensate

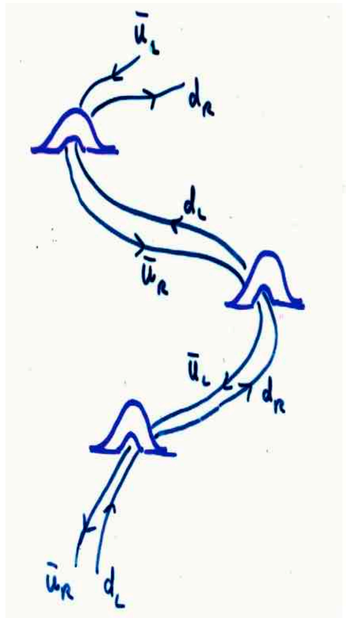

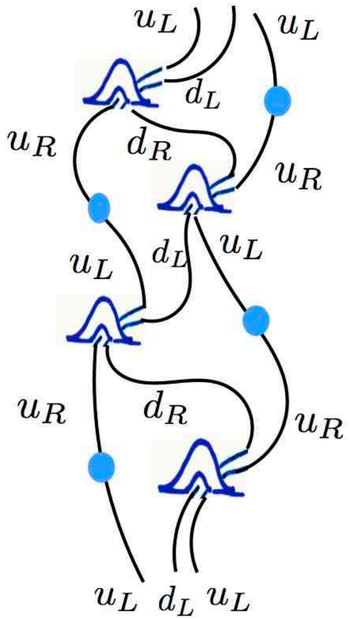

"molecular component"
which is denser
because overlapping
I and bar-I
has smaller action
but without near-zero
Dirac eigenvalues!

Ilgenfritz,ES 1988,1993

current lattice studies with G^2,G^3 observables and gradient flow cooling (extrapolated to zero time) suggest kappa=O(1)

in the ff plots we used kappa=1
and this gets the data!

- A. Athenodorou, P. Boucaud, F. De Soto, J. Rodr´ıguez-Quintero, and S. Zafeiropoulos JHEP 02, 140 (2018), arXiv:1801.10155 [hep-lat].

- **Careful study of "cooling" by gradient flow**

size

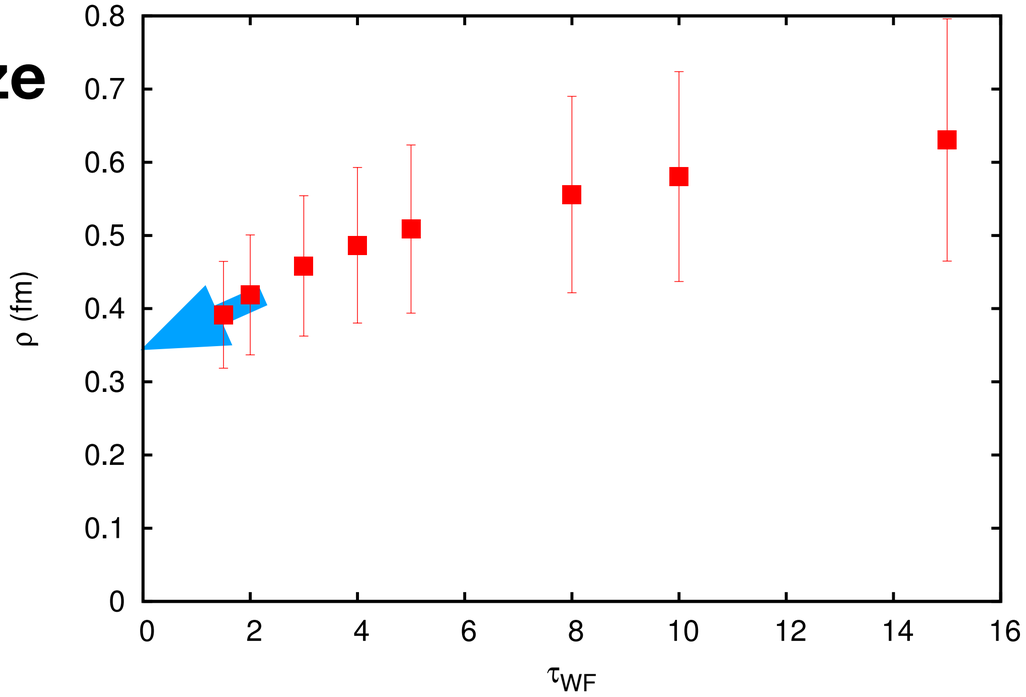

cooling time

density

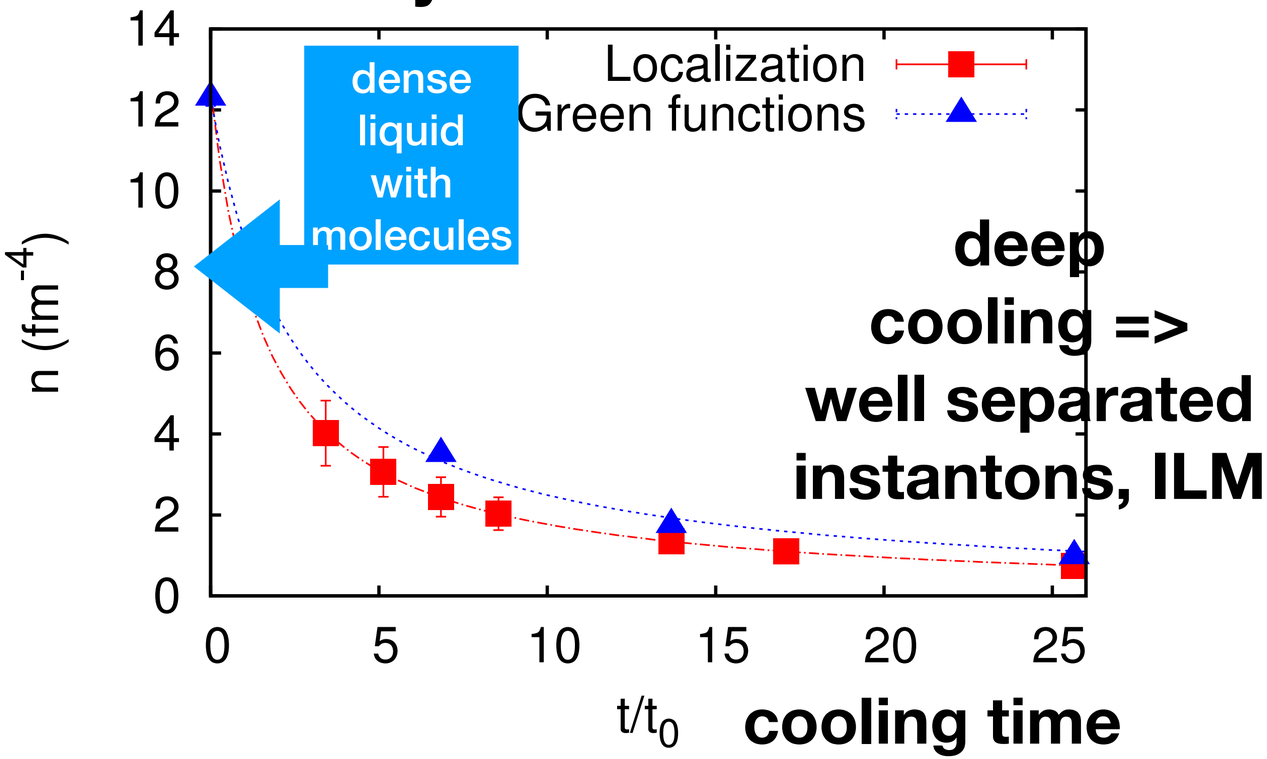

deep cooling => well separated instantons, ILM

cooling time

Nonperturbative central potential in ILM

$$n_{mol} + n_I + n_{\bar{I}} = 7.\,\mathrm{fm}^{-4} \qquad R_{dense} \equiv n^{-1/4} = 0.61\,fm \approx 2\rho$$

instanton-induced is as good as Cornell potential for many mesons, e.g.

$$\Upsilon[1S], \eta_b[1S], \Upsilon[2S], \Upsilon[3S], \Upsilon[4S]$$

but for bb states with N>4 or ligher quark states, still one has to use linear for r> 1 fm

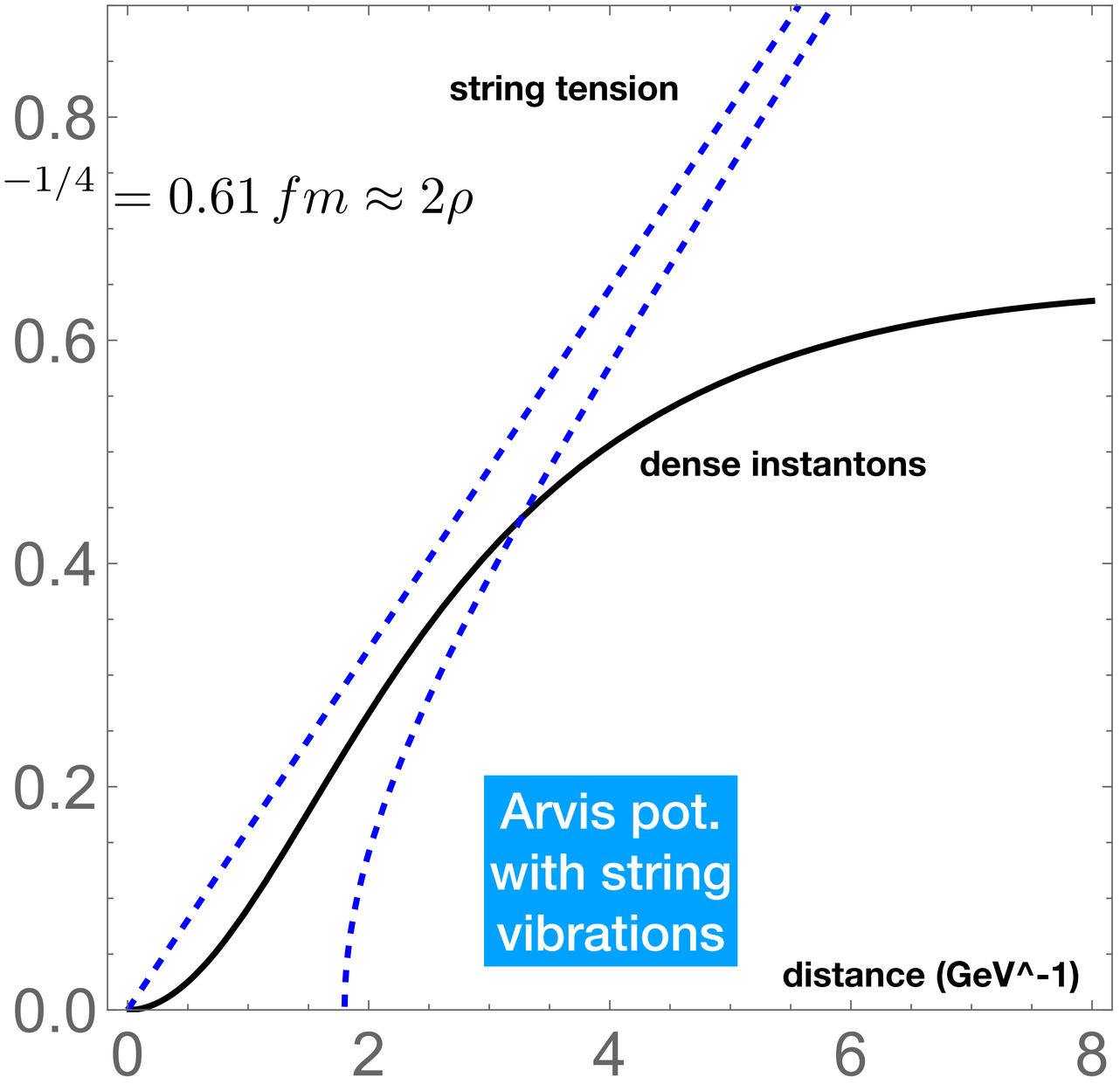

Strongly correlated pairs or molecules:

remain there at T>Tc

`streamline equation"

solved numerically

used to calculate sphaleron production

[Ilgenfritz and Shuryak, 1989].

[Balitsky and Yung, 1986],

[Verbaarschot, 1991].

Shuryak and Verbaarschot, 1992]

[Shuryak and Zahed, 2021

$$A^{\mu a}(x)=\frac{\bar{\eta}^{a\mu\nu}y_I^\nu\rho^2/Y_I^2+\eta^{a\mu\nu}y_A^\nu\rho^2/Y_A^2}{1+\rho^2/Y_A+\rho^2/Y_I},$$

strong fields, O(few GeV^2)

action density G^2

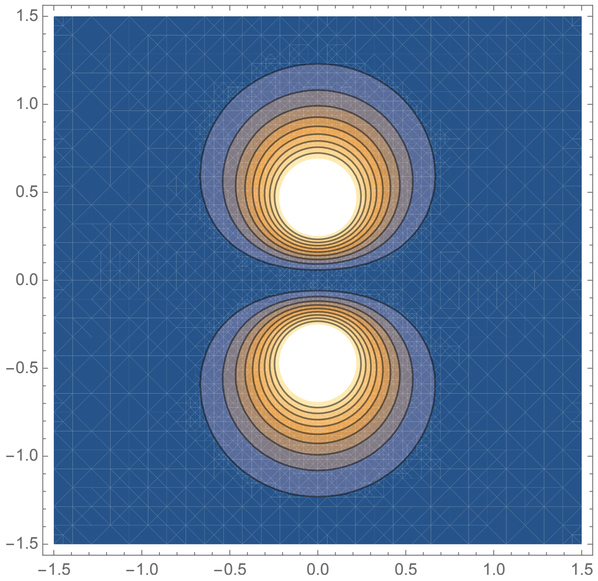

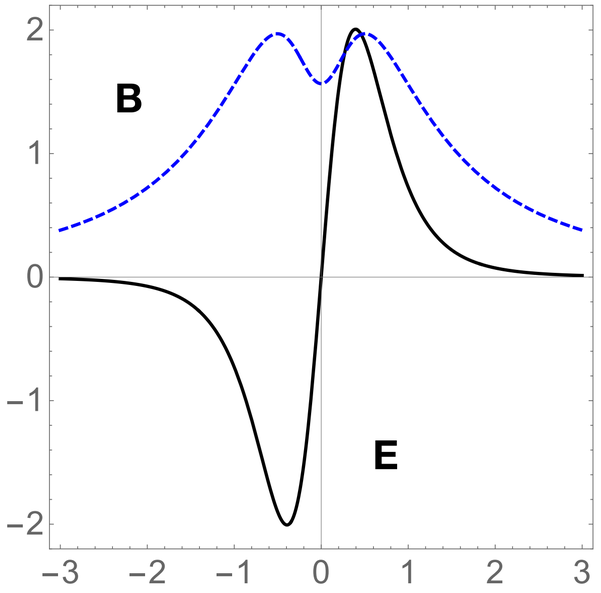

relativistic corrections to order 1/M^2 have in genral 5 potentials
3 spin-dependent potentials
spin-spin, spin-orbit and tensor

E. Eichten and F. Feinberg, "Spin Dependent Forces in QCD," Phys. Rev. D **23**, 2724 (1981

the corresponding potentials are given by Wilson lines decorated by field strength insertions

Here is the main point: electric flux tubes models do not give predictions for magnetic fields

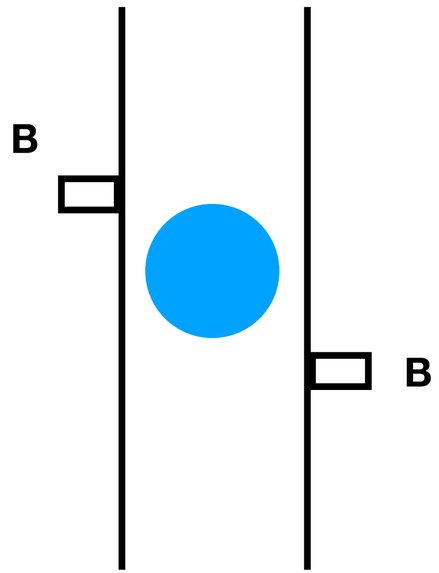

flux tube is electric spins interact with magnetic field

instantons on the other hand are selfdual E=B

Instanton effects in spin-related potentials

Wilson lines complemented by two field strengths => in general, 5 potentials for instantons related to Vc

E. Eichten and F. Feinberg, "Spin Dependent Forces in QCD," Phys. Rev. D **23**, 2724 (1981

$$V_{SD} = \left(\frac{S_Q \cdot L_Q}{2m_Q^2} - \frac{S_{\bar{Q}} \cdot L_{\bar{Q}}}{2m_{\bar{Q}}^2}\right)\left(\frac{1}{r}\frac{d}{dr}\left(V(r) + 2V_1(r)\right)\right)$$
$$+\left(\frac{S_{\bar{Q}} \cdot L_Q}{m_Q m_{\bar{Q}}} - \frac{S_Q \cdot L_{\bar{Q}}}{m_{\bar{Q}} m_{\bar{Q}}}\right)\left(\frac{1}{r}\frac{d}{dr}V_2(r)\right)$$
$$+\frac{(3S_Q \cdot \hat{r} S_{\bar{Q}} \cdot \hat{r} - S_Q \cdot S_{\bar{Q}})}{3m_Q m_{\bar{Q}}}V_3(r) + \frac{1}{3}\frac{S_Q \cdot S_{\bar{Q}}}{m_Q m_{\bar{Q}}}V_4(r)$$

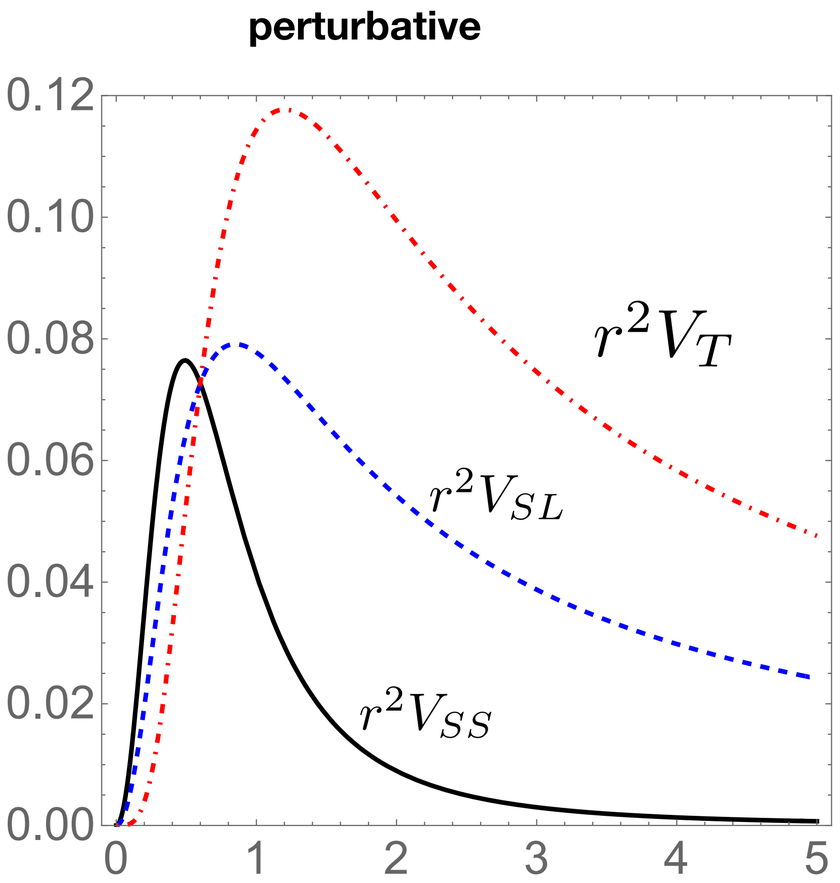

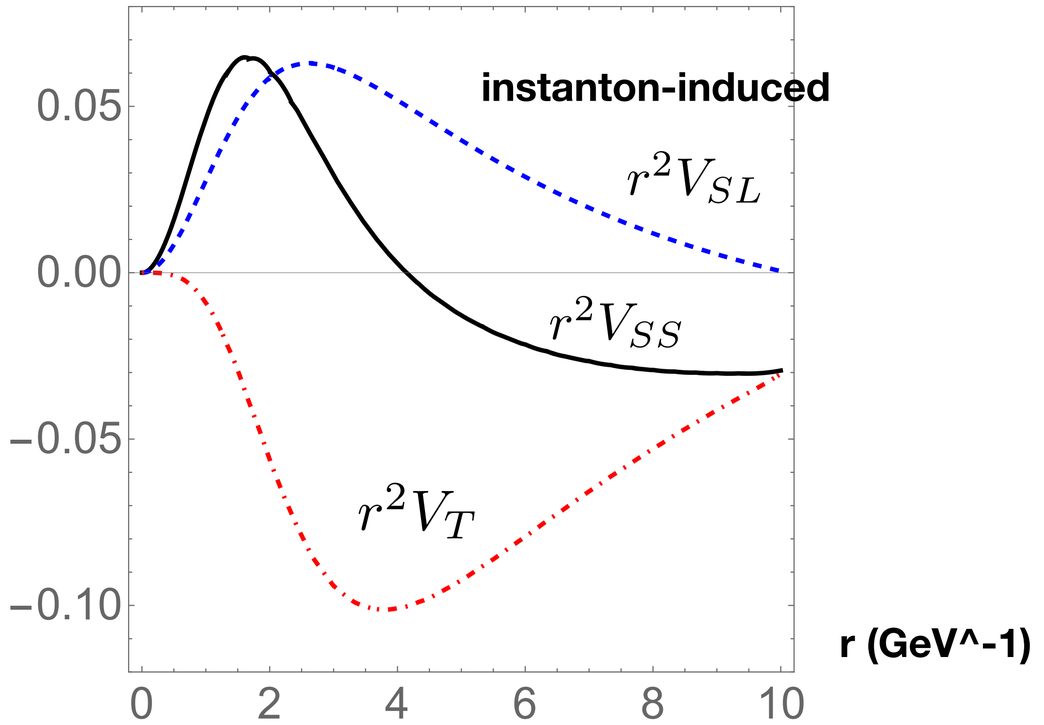

Their sum explains lattice data for Vss and explains spin splittings rather well, except in light-light mesons

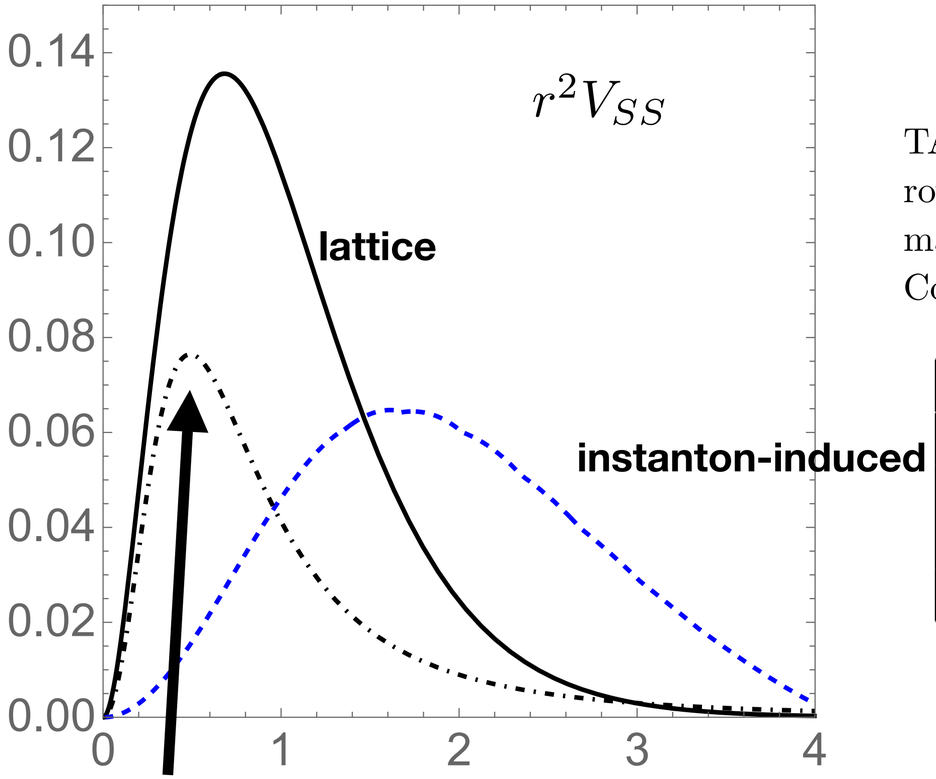

smeared delta function normalized to Coulomb

TABLE II. "Hyperfine" splittings of certain $L = 0$ mesons with $J = 1$ and $J = 0$. The first row of numbers shows the experimental values (MeV) (rounded to 1 MeV). The second gives matrix elements of the lattice-based spin-spin potential (19), the next two are those for (regulated) Coulomb and instanton-induced spin-spin forces.

flavors	$M_\Upsilon - M_{\eta_b}$	$M_{J/\psi} - M_{\eta_c}$	$M(D^*) - M(D)$	$M(K^*) - M(K)$	$M(\rho) - M(\pi)$
Exp	61.	116.	137.	398.	636.
$\langle V_{SS}^{lat}/3M_1M_2\rangle$	46.	108.	98.	170.	
$\langle\vec{\nabla}^2V_C/3M_1M_2\rangle$	28.	58.	48.	82.	
$\langle\vec{\nabla}^2V_{inst}/3M_1M_2\rangle$	7.	30.	48.	90.	

another type of instanton effect due to t'Hooft Lagrangian

adds 40 MeV all three explain the observed splitting

massless pion is due to zero modes (t' Hooft Lagrangian)

we also studied splittings of 1P states h,chi_0,chi_1,chi_2 and calculated matrix elements of VSS,VSL,VT also

The color force acting on a quark in the pion and nucleon

Wei-Yang Liu,* Edward Shuryak,† and Ismail Zahed‡

The most interesting correlation between partons are those stemming from a polarized target. While the structure function $g_1(x, Q^2)$ starts with the usual twist-2 operators, the structure function $g_2(x, Q^2)$ starts with twist-3. Since in experiments the structure functions can be separated *kinematically*, this fact offers the most direct access to the higher twist physics. For a transversely polarized nucleon, at 90^0 to the incoming momentum, $g_1(x, Q^2)$ vanishes and the remaining DIS amplitude is purely twist-3. The pertinent physics is related with the local operator[1]

$$O_{\bar{q}Gq} = ig\big(\bar{q}\gamma^\rho G^{\mu\nu} q\big) \tag{1}$$

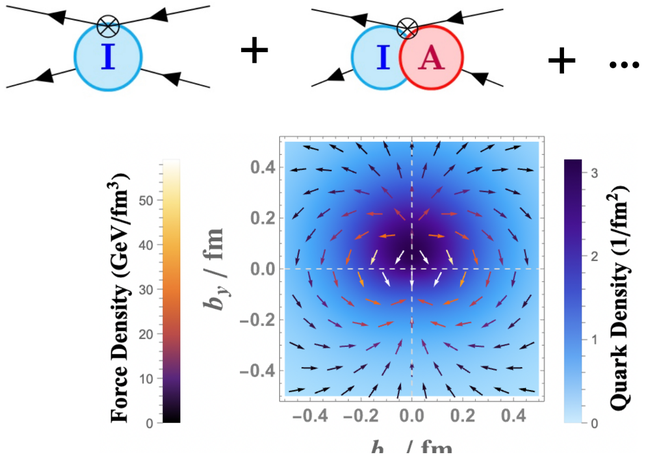

lattice

J. A. Crawford, K. U. Can, R. Horsley, P. E. L. Rakow, G. Schierholz, H. Stüben, R. D. Young, and J. M. Zanotti, "Transverse force distributions in the proton from lattice QCD," (2024), arXiv:2408.03621 [hep-lat].

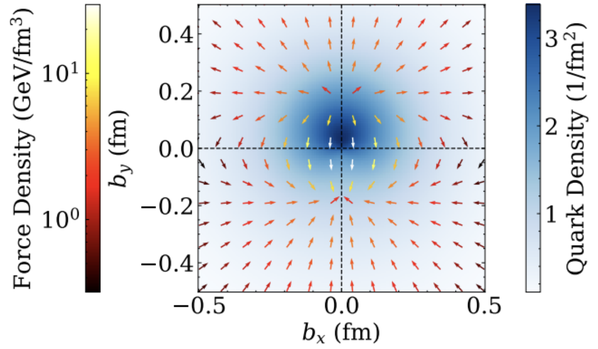

Edward V. Shuryak and A. I. Vainshtein, "Theory of Power Corrections to Deep Inelastic Scattering in Quantum Chromodynamics. 2. Q**4 Effects: Polarized Target," Nucl. Phys. B **201**, 141 (1982).

Summary

1. **Jacobi coordinates used, both in CM and LF spectroscopy: no fake variables**
2. **LF mesons, baryons ... pentaquarks quantized in momentum representation**
3. **all defined on proper manifolds**
4. **basic model: constituent quark+confinement, in N diquark correlations**
5. **Novel methods to enforce Fermi statistics, used for 5,6 and more light quarks**
6. **spin problem + antiquark PDFs from pentaquark admixture to nucleons**

1. Topological landscape, sphalerons and instantons
2. Instanon-based forces, 't Hooft Lagrangian
3. Instanton liquid model
4. Chiral symmetry breaking
5. instanton-antiinstanton molecules
6. generation of interquark potentials
7. spin-dependent forces

unquenching program: tetraquarks, pentaquarks and hybrids